



Four years of Ulysses dust data: 1996–1999

H. Krüger^{a,*}, E. Grün^a, M. Landgraf^b, S. Dermott^c, H. Fechtig^a, B.A. Gustafson^c, D.P. Hamilton^d,
M.S. Hanner^e, M. Horányi^f, J. Kissel^g, B.A. Lindblad^h, D. Linkert^a, G. Linkert^a, I. Mann^{i,k},
J.A.M. McDonnell^j, G.E. Morfill^g, C. Polanskey^e, G. Schwehm^k, R. Srama^a, H.A. Zook^{l, 1}

^aMax-Planck-Institut für Kernphysik, Post 69029 Heidelberg, Germany

^bESOC, 64293 Darmstadt, Germany

^cUniversity of Florida, Gainesville, FL 32611, USA

^dUniversity of Maryland, College Park, MD 20742-2421, USA

^eJet Propulsion Laboratory, Pasadena, CA 91109, USA

^fLaboratory for Atmospheric and Space Physics, University of Colorado, Boulder, CO 80309, USA

^gMax-Planck-Institut für Extraterrestrische Physik, 85748 Garching, Germany

^hLund Observatory, 221 Lund, Sweden

ⁱInstitut für Planetologie, Universität Münster, 48149 Münster, Germany

^jPlanetary and Space Science Research Institute, The Open University, Milton Keynes, MK7 6AA, UK

^kESTEC, 2200 AG Noordwijk, Netherlands

^lNASA Johnson Space Center, Houston, TX 77058, USA

Received 5 January 2001; received in revised form 15 May 2001; accepted 15 May 2001

Abstract

The Ulysses spacecraft is orbiting the Sun on a highly inclined ellipse ($i = 79^\circ$, perihelion distance 1.3 AU, aphelion distance 5.4 AU). Between January 1996 and December 1999 the spacecraft was beyond 3 AU from the Sun and crossed the ecliptic plane at aphelion in May 1998. In this 4-yr period 218 dust impacts were recorded with the dust detector on board. We publish and analyse the complete data set of both raw and reduced data for particles with masses 10^{-16} – 10^{-8} g. Together with 1477 dust impacts recorded between launch of Ulysses and the end of 1995 published earlier (Grün et al., *Planet. Space Sci.* 43 (1995a) 971; Krüger et al., *Planet. Space Sci.* 47 (1999b) 363), a data set of 1695 dust impacts detected with the Ulysses sensor between October 1990 and December 1999 is now available. The impact rate measured between 1996 and 1999 was relatively constant with about 0.2 impacts per day. The impact direction of the majority of the impacts is compatible with particles of interstellar origin, the rest are most likely interplanetary particles. The observed impact rate is compared with a model for the flux of interstellar dust particles. The flux of particles several micrometres in size is compared with the measurements of the dust instruments on board Pioneer 10 and Pioneer 11 beyond 3 AU (Humes, *J. Geophys. Res.* 85 (1980) 5841). Between 3 and 5 AU, Pioneer results predict that Ulysses should have seen 5 times more ($\sim 10 \mu\text{m}$ sized) particles than actually detected. © 2001 Published by Elsevier Science Ltd.

1. Introduction

Ulysses is the first interplanetary spaceprobe which left the ecliptic plane of our Solar System and flew over the Sun's poles. The craft's orbital plane is almost perpendicular to the ecliptic plane with an aphelion as far from the Sun as Jupiter. The main scientific objectives of the mission are

the exploration of the Sun at high heliographic latitudes, investigation of the solar wind and the interplanetary medium as well as interstellar gas and cosmic rays.

The Ulysses spacecraft is equipped with a highly sensitive impact ionisation dust detector which measures in situ impacts of micrometre and sub-micrometre dust grains. The detector is practically identical with the dust instrument on board the Galileo spaceprobe. Both dust instruments have been described in previous publications (Grün et al., 1992a, b, 1995c).

In the following we give a brief overview and an update of the most important scientific achievements of the Ulysses dust measurements. References to other works related to

* Corresponding author. Tel.: +49-6221-516-563;

fax: +49-6221-516-324.

E-mail address: harald.krueger@mpi-hd.mpg.de (H. Krüger).

¹ Passed away on 14 March 2001.

Ulysses and Galileo measurements on dust in the Jovian system, interstellar dust in the heliosphere and on the interplanetary meteoroid complex are given in various earlier publications (Grün et al., 1995a, b; Krüger et al., 1999a, b). For comprehensive reviews of the scientific achievements of the Ulysses mission, including those from the dust investigations, the reader is referred to *The heliosphere at solar minimum: The Ulysses perspective* (Balogh et al., 2001) and the chapter on dust by Grün et al. (2001) in the same book.

With the Ulysses dust instrument burst-like intermittent streams of tiny dust grains were discovered in interplanetary space (Grün et al., 1993) which had been emitted from the Jovian system (Zook et al., 1996). These grains strongly interact with the interplanetary and the Jovian magnetic fields (Horányi et al., 1997; Grün et al., 1998). After an ongoing debate about the origin of these grains (Io, Jupiter's gossamer ring, etc., Hamilton and Burns, 1993; Horányi et al., 1993), Io was recently confirmed as their ultimate source (Graps et al., 2000).

Ulysses and Galileo dust measurements have been used to derive the three-dimensional distribution of the interplanetary dust complex and their relation to the underlying populations of parent bodies like asteroids and comets (Divine, 1993; Grün et al., 1997). Studies of asteroidal dust released from the IRAS dust bands show that they are not efficient enough dust sources to maintain a stable interplanetary dust cloud (Mann et al., 1996). Recently, the properties of β meteoroids (i.e. dust particles which leave the Solar System on unbound orbits due to acceleration by radiation pressure) have been studied with the Ulysses dust data set (Wehry and Mann, 1999).

Another discovery made with the Ulysses detector were interstellar particles sweeping through the Solar System (Grün et al., 1993). The grains were identified by their impact direction and impact velocities, the latter being compatible with particles moving on hyperbolic heliocentric trajectories (Grün et al., 1994). Their dynamics depend on grain size and are strongly affected by the interaction with the heliosphere and by solar radiation pressure (Mann and Kimura, 2000; Landgraf, 2000). This has a strong influence on the size distribution and fluxes of grains measured inside the heliosphere. The mass distribution of grains measured at heliocentric distances inside 4 AU shows a lack of grains with masses $\sim 10^{-13}$ g: particles for which the ratio between the solar radiation force and the gravitational force, β , exceeds unity are rejected from the Sun and thus hindered from entering the inner Solar System (β gap; Landgraf et al., 1999). This in turn allows to infer optical properties of the grains which are consistent with different models of dust composition and structure.

Ulysses and Galileo in situ measurements imply that the intrinsic size distribution of interstellar grains in the local interstellar medium extends to grain sizes larger than those detectable by astronomical observations (Frisch et al., 1999; Landgraf et al., 2000; Grün and Landgraf, 2000). The ex-

istence of such 'big' interstellar grains is also indicated by observations of radar meteors entering the Earth's atmosphere (Taylor et al., 1996; Baggaley, 2000). The dust-to-gas mass ratio in the local interstellar cloud is several times higher than the standard interstellar value derived from cosmic abundances, implying the existence of inhomogeneities in the diffuse interstellar medium on relatively small length scales.

This is the seventh paper in a series dedicated to presenting both raw and reduced data obtained from the dust instruments on board the Ulysses and Galileo spacecraft. The reduction process of Ulysses and Galileo dust data has been described by Grün et al. (1995c, hereafter Paper I). In Papers III and V (Grün et al., 1995a; Krüger et al., 1999b) we present the Ulysses data set spanning the 5 yr time period from October 1990 to December 1995. Papers II and IV (Grün et al., 1995b; Krüger et al., 1999a) discuss the 6 years of Galileo data from October 1989 to December 1995. The current paper extends the Ulysses data set from January 1996 until December 1999, and a companion paper (Krüger et al., 2001) (Paper VI) presents Galileo's 1996 measurements.

The main data products are a table of the impact rate of all impacts determined from the particle accumulators and a table of both raw and reduced data of all dust impacts for which the full data set of measured impact parameters has been transmitted to Earth. The information presented in these papers is similar to data which we are submitting to the various data archiving centres (Planetary Data System, NSSDC, Ulysses Data Centre). Electronic access to the data is also possible via the world wide web: <http://www.mpi-hd.mpg.de/dustgroup/>.

This paper is organised like Papers III and V. We begin with an overview of important events of the Ulysses mission between 1996 and 1999 (Section 2). Sections 3 and 4 describe and analyse the Ulysses dust data set for this period. In Section 5, we discuss the properties of different populations of interplanetary and interstellar dust in the data set and compare our Ulysses measurements with dust fluxes measured in the outer Solar System with the Pioneer 10 and 11 spacecraft. In Section 6, we summarise our conclusions. An appendix gives a conversion between impact charges as measured by the dust instrument and grain masses and sizes for different impact speeds.

2. Mission and instrument operation

2.1. Ulysses mission and dust instrument characteristics

The Ulysses spacecraft was launched on 6 October 1990. A swing-by manoeuvre at Jupiter in February 1992 rotated the orbital plane 79° relative to the ecliptic plane. On the resulting trajectory (Fig. 1) Ulysses passed under the south pole of the Sun (October 1994), crossed the ecliptic plane at a perihelion distance of 1.3 AU (March 1995) and passed

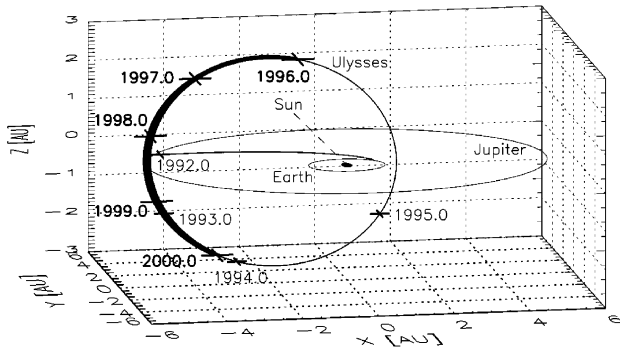


Fig. 1. The trajectory of Ulysses in ecliptic coordinates. The Sun is in the centre. The orbits of Earth and Jupiter indicate the ecliptic plane. The initial trajectory of Ulysses was in the ecliptic plane. Since Jupiter flyby in early 1992 the orbit has been almost perpendicular to the ecliptic plane (79° inclination). Crosses mark the spacecraft position at the beginning of each year. The 1996–1999 part of the trajectory is shown as a thick line. Vernal equinox is to the right (positive x -axis).

Table 1

Numerical values of the orbital elements for the Ulysses trajectory (<http://helio.estec.esa.nl/Ulysses/>)^a

$a = 3.3730032 AU (504594094 \text{ km})$
$e = 0.60306$
$i = 79.12801^\circ$
$\Omega = -22.51862^\circ$
$w = -1.11377^\circ$
$M = 0.1591096 (J - 2449788.986)^\circ$

^aThe reference frame is the mean ecliptic and equinox of 1950.0. a is the semi-major axis, i the inclination, e the eccentricity, Ω the longitude of ascending node measured from the vernal equinox, w the argument of perihelion and M the mean anomaly of the orbit. J is the Julian date of interest.

over the Sun's north pole (August 1995). In April 1998, the spacecraft finished its first out-of-ecliptic orbit and crossed the ecliptic plane again at an aphelion distance of 5.4 AU. In 2000 and 2001, it will make its second pass over the Sun's polar regions. Orbital elements for the out-of-ecliptic part of the Ulysses trajectory are given in Table 1.

Ulysses spins at five revolutions per minute about the centreline of its high gain antenna which normally points at Earth. Fig. 2 shows the deviation of the spin axis from the Earth direction for the period 1996–1999. Most of the time the spin axis pointing was within 0.5° of the nominal Earth direction. This small deviation is usually negligible for the analysis of measurements with the dust detector. The Ulysses spacecraft and mission are explained in more detail by Wenzel et al. (1992). Details about the data transmission to Earth can also be found in Paper III.

The Ulysses dust detector (GRU) has a 140° wide field of view and is mounted at the spacecraft nearly at right angles (85°) to the antenna axis (spacecraft spin axis). Due to this mounting geometry, the dust sensor is most sensitive to particles approaching from the plane perpendicular to

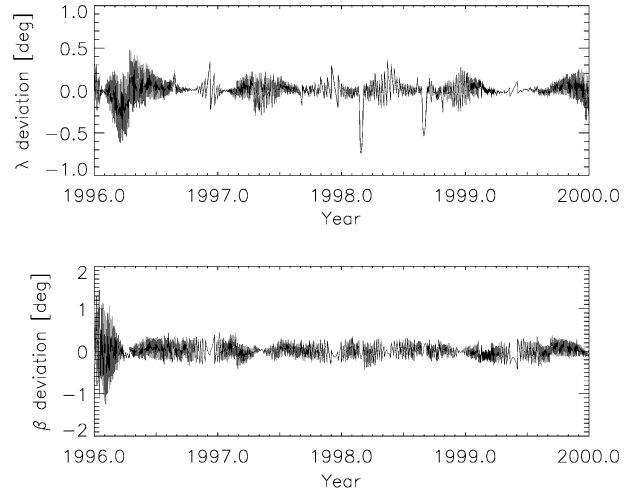


Fig. 2. Spacecraft attitude: deviation of the antenna pointing direction (i.e. positive spin axis) from the nominal Earth direction. The angles are given in ecliptic longitude (top) and latitude (bottom, equinox 1950.0).

the spacecraft–Earth direction. The impact direction of dust particles is measured by the rotation angle which is the sensor viewing direction at the time of a dust impact. During one spin revolution of the spacecraft the rotation angle scans through a complete circle of 360° . Zero degrees rotation angle is defined to be the direction closest to ecliptic north. At high ecliptic latitudes, however, the sensor pointing at 0° rotation angle significantly deviates from the actual north direction. During the passages over the Sun's polar regions the sensor always scans through a plane tilted by about 30° from the ecliptic and all rotation angles lie close to the ecliptic plane (cf. Fig. 4 in Grün et al., 1997). A sketch of the viewing geometry around aphelion passage can be found in Grün et al. (1993).

Table 2 gives significant mission and dust instrument events from 1996 to 1999. Earlier events are only listed if especially significant. A comprehensive list of events from launch until the end of 1995 is given in Papers III and V.

2.2. Instrumental noise

Analysis of the in-orbit noise characteristics of the dust instrument (Paper III) led to a relatively noise-free configuration with which the instrument has been normally operated so far: channeltron voltage 1140 V ($HV=3$); event definition status such that either the channeltron or the ion-collector channel can, independent of each other, start a measurement cycle ($EVD=C,I$); detection thresholds for ion-collector, channeltron and electron-channel set to the lowest levels and the detection threshold for the entrance grid set to the first digital step ($SSEN=0,0,0,1$). See Paper I for a description of these terms. This instrument set up is hereafter called nominal configuration.

Dedicated noise tests were performed at about 1 month intervals to monitor instrument health and noise

Table 2

Ulysses mission and dust detector (GRU) configuration, noise tests and other events. Only selected events are given before 1996. See Section 2 for details^a

Yr-day	Date	Time	Event
90-279	06.10.90		Ulysses launch
92-039	08.02.92	12:04	Ulysses Jupiter closest approach
95-300	27.10.95	16:23	GRU heater: 1200 mW
95-346	12.12.95	08:54	GRU nominal configuration: HV=3, EVD=C,I, SSEN=0001
96-011	11.01.96	05:59	GRU noise test
96-040	09.02.96	05:00	GRU noise test
96-067	07.03.96	21:00	GRU noise test
96-096	05.04.96	20:00	GRU noise test
96-123	02.05.96	15:59	GRU noise test
96-151	30.05.96	20:59	GRU noise test
96-180	28.06.96	13:00	GRU noise test
96-207	25.07.96	10:00	GRU noise test
96-230	17.08.96	16:00	Ulysses DNEL # 7
96-231	18.08.96	01:28	GRU on
96-233	20.08.96	01:02	GRU nominal configuration
96-237	24.08.96	09:00	GRU noise test
96-263	19.09.96	16:59	GRU noise test
96-291	17.10.96	05:59	GRU noise test
96-319	14.11.96	11:59	GRU noise test
96-347	12.12.96	03:00	GRU noise test
97-009	09.01.97	05:59	GRU noise test
97-037	05.02.97	00:00	GRU noise test
97-065	06.03.97	01:00	GRU noise test
97-091	01.04.97	20:55	Ulysses DNEL # 8
97-092	02.04.97	05:21	GRU on
97-093	03.04.97	03:29	GRU nominal configuration
97-093	03.04.97	18:59	GRU noise test
97-121	01.05.97	03:00	GRU noise test
97-149	29.05.97	00:00	GRU noise test
97-177	26.05.97	00:00	GRU noise test
97-205	24.07.97	17:00	GRU noise test
97-233	21.08.97	08:00	GRU noise test
97-261	18.09.97	06:00	GRU noise test
97-290	17.10.97	04:00	GRU noise test
97-317	13.11.97	04:00	GRU noise test
97-345	11.12.97	01:16	GRU noise test
98-008	08.01.98	03:59	GRU noise test
98-036	05.02.98	09:22	GRU noise test
98-064	05.03.98	05:00	GRU noise test
98-092	02.04.98	02:00	GRU noise test
98-110	20.04.98		Ulysses aphelion passage (5.4 AU)
98-120	30.04.98	19:59	GRU noise test
98-129	09.05.98		Ulysses ecliptic plane crossing (5.4 AU)
98-148	28.05.98	17:59	GRU noise test
98-176	25.06.98	17:00	GRU noise test
98-204	23.07.98	10:00	GRU noise test
98-232	20.08.98	08:00	GRU noise test
98-260	17.09.98	00:00	GRU noise test
98-288	15.10.98	00:00	GRU noise test
98-318	14.11.98	08:00	GRU noise test
98-344	10.12.98	16:00	GRU noise test
99-007	07.01.99	16:30	GRU noise test
99-035	04.02.99	13:00	GRU noise test
99-046	15.02.99	10:45	Ulysses DNEL # 9
99-047	16.02.99	00:01	GRU on
99-048	17.02.99	04:29	GRU nominal configuration
99-064	05.03.99	14:00	GRU noise test
99-092	02.04.99	12:00	GRU noise test
99-119	29.04.99	10:00	GRU noise test
99-147	27.05.99	06:00	GRU noise test
99-175	24.06.99	06:00	GRU noise test
99-203	22.07.99	01:00	GRU noise test
99-232	20.08.99	03:00	GRU noise test
99-260	17.09.99	00:00	GRU noise test
99-287	14.10.99	01:00	GRU noise test
99-315	11.11.99	17:00	GRU noise test
99-343	09.12.99	16:00	GRU noise test

^a Abbreviations used: DNEL, Disconnect non-essential loads (i.e. all scientific instruments); HV, channeltron high voltage step; EVD, event definition, ion- (I), channeltron- (C), or electron-channel (E); SSEN, detection thresholds, ICP, CCP, ECP and PCP.

characteristics. During all these tests the operational configuration was changed in four steps at 1-h intervals, starting from the nominal setting described above: (a) set the event definition status such that the channeltron, the ion collector and the electron-channel can initiate a measurement cycle ($EVD = C, I, E$); (b) set the thresholds for all channels to their lowest levels ($SSEN = 0, 0, 0, 0$); (c) reset the event definition status to its nominal configuration ($EVD = C, I$) and increase the channeltron high voltage by one digital step ($HV = 4$); (d) reset the instrument to its nominal operational configuration (channeltron high voltage to $HV = 3$, detection thresholds to $SSEN = 0, 0, 0, 1$).

The noise tests revealed a long-term drop of the noise sensitivity of the instrument: in step (c), when the channeltron high voltage was increased, fewer noise events were triggered compared to the earlier period before 1996. This is most likely caused by a reduction in the channeltron amplification due to ageing (see also Section 3) although less noise is generally expected far away from the Sun. In addition, the average charge amplitudes measured at the target during noise events were reduced. This is probably an effect of degradation of the instrument electronics.

The noise response of the Ulysses dust detector will be continuously monitored in the future to maintain stable instrument operation. So far, the degradation does not lead to a serious reduction in the instrument sensitivity: although we expect a lower number of class 3 events due to the reduced channeltron amplification, the dust impacts causing these events should show up as class 0 impacts.

From 1996 to 1999 three spacecraft anomalies occurred during which all scientific instruments on board Ulysses were switched off automatically. These disconnections of all non-essential loads are called DNELs for short. Within about 2 days after each DNEL, the dust instrument was switched on again and reconfigured to its nominal operational mode. The resulting loss of continuous measurement time with the dust instrument is negligible.

Two heaters allow for a relatively stable operating temperature of the dust sensor (heating powers 400 and 800 mW, respectively). Both heaters were switched on during the time period 1996–1999 considered here, providing a constant heating power of 1200 mW. Sensor heating was necessary because the spacecraft was outside 3 AU all the time and hence received relatively little radiation from the Sun. During DNELs the heaters were switched off, but switched on again several hours before the instrument was reconfigured so that a stable operating temperature could be achieved at switch-on to avoid instrument damage. From 1996 to 1999 the temperature of the dust sensor was between -10°C and -23°C which is within the specified operational range. A switch-off of the 400 mW heater planned for September 1999 for power saving reasons on board the spacecraft did not become necessary. Due to a decreasing power output of the radioisotope batteries (RTGs) power saving issues will become important for instrument operation on board Ulysses after 2001.

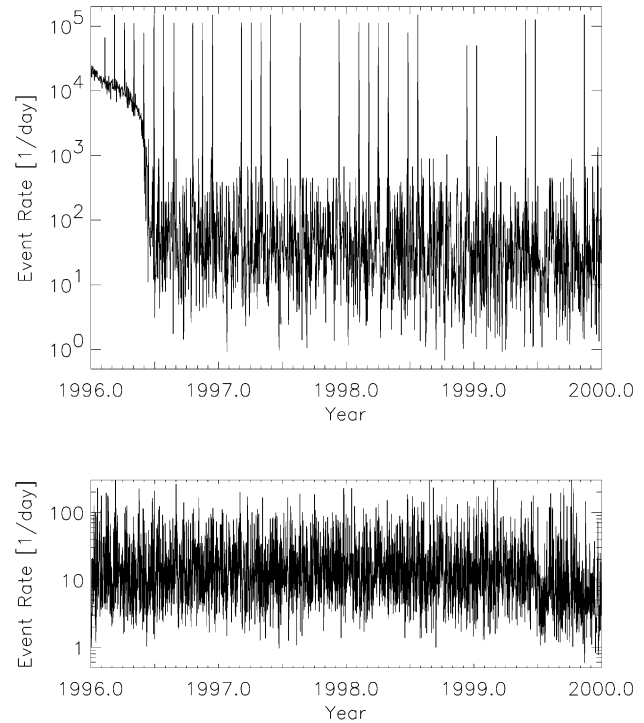


Fig. 3. Noise rate (class 0 events) detected with the dust instrument. Upper panel: Daily maxima in the noise rate (determined from the AC01 accumulator). The sounder was operated for only 2% of the total time, and the daily maxima are dominated by sounder noise. Sharp spikes are caused by periodic noise tests and short periods of reconfiguration after DNELs (Table 2). Lower panel: Noise rate detected during quiet intervals when the sounder was switched off, which was the case about 98% of the time. The curve shows a 1-day average calculated from the number of AC01 events for which the complete information has been transmitted to Earth.

Fig. 3 shows the noise rate of the dust instrument for the 1996–1999 period. The upper panel shows the daily maxima of the noise rate. They are dominated by noise caused by interference with the sounder of the Unified Radio and Plasma wave instrument (URAP) on board Ulysses (Stone et al., 1992). The sounder is typically operated for periods of only 2 min with quiet intervals of about 2 h. Thus, the high noise rates caused by the sounder occurred only during about 2% of the total time. The remaining 98% are free of sounder noise. The noise rates measured during sounder operation are correlated with the distance to, and the position of, the Sun with respect to the sensor-viewing direction (Baguhl et al., 1993). Most noise events were triggered when the Sun shone directly into the sensor. Strong sounder noise occurred in 1994 and 1995 while Ulysses was within about 3 AU heliocentric distance (Paper V) and this continued until mid-1996 (Fig. 3, upper panel). In this time period the sounder noise was sufficiently high to cause significant dead time in the dust instrument during the time intervals of sounder operation.

When the spacecraft was at a large heliocentric distance, the noise rate was very low even during periods of

sounder operation. This was the case after mid-1996. Individual sharp spikes in the upper panel of Fig. 3 are caused by noise tests which occurred at monthly intervals. After mid-1996 many of these noise tests did not show up in the diagram anymore because of degrading of the channeltron led to a reduced noise sensitivity of the instrument (see also Section 4).

The sounder was operated frequently during noise tests. In step (c) of the noise test (channeltron high voltage increased) with simultaneous sounder operation, the noise signals usually showed a channeltron charge amplitude $CA = 1$ (digital units) between 1991 and 1996. Later in the mission, values of $CA = 0$ dominated which is also indicative of a channeltron degradation.

The noise rates when the sounder was switched off are shown in the lower panel of Fig. 3. The average was about 10 events per day and this was random noise not related to the sounder. Dead time is negligible during these periods.

3. Impact events

Impact events are classified into four classes and six ion charge amplitude ranges which lead to 24 individual categories. In addition, the instrument has 24 accumulators with one accumulator belonging to one individual category. Class 3, our highest class, are real dust impacts and class 0 are mostly noise events. Depending upon the noise of the charge measurements, classes 1 and 2 can be true dust impacts or noise events. This classification scheme for impact events has been described in Paper I and the scheme is still valid for the Ulysses dust instrument. In contrast to the Galileo dust instrument which had to be reprogrammed because of the low data transmission capabilities of the Galileo spacecraft, no such reprogramming has been necessary for Ulysses so far. Most of the data processing for Ulysses can be done on the ground.

Between 1 January 1996 and 31 December 1999 the complete data sets (sensor orientation, charge amplitudes, charge rise times, etc.) of 16,758 events including 218 dust impacts were transmitted to Earth. Table 3 lists the number of all dust impacts counted with the 24 accumulators of the dust instrument. ‘AC xy ’ refers to class number ‘ x ’ and amplitude range ‘ y ’ (for a detailed description of the accumulator categories see Paper I). As discussed in the previous section, most noise events were recorded during the short time periods when either the sounder of the URAP instrument was operating (Paper III) or when the dust instrument was configured to its high sensitive state for noise tests, or both. During these periods many events were only counted by one of the 24 accumulators because their full information was overwritten before the data could be transmitted to Earth. Since the dust impact rate was low during times outside these periods, it is expected that only the data sets of very few true dust impacts were lost.

All 218 dust impacts detected from 1996 to 1999 for which the complete information exists are listed in Table 4. Dust particles are identified by their sequence number and their impact time (first two columns). The event category—class (CLN) and amplitude range (AR)—are given in the third and fourth columns. Raw data as transmitted to Earth are shown in the next columns: sector value (SEC) which is the spacecraft spin orientation at the time of impact, impact charge numbers (IA, EA, CA) and rise times (IT, ET), time difference and coincidence of electron and ion signals (EIT, EIC), coincidence of ion and channeltron signal (IIC), charge reading at the entrance grid (PA) and time (PET) between this signal and the impact. Then the instrument configuration is given: event definition (EVD), charge sensing thresholds (ICP, ECP, CCP, PCP) and channeltron high voltage step (HV). Compare Paper I for further explanation of the instrument parameters.

The next four columns in Table 4 give information about Ulysses’ orbit: heliocentric distance (R), ecliptic longitude and latitude (LON, LAT) and distance from Jupiter (D_{Jup} , in astronomical units). The next column gives the rotation angle (ROT) as described in Section 2. Then follows the pointing direction of the dust instrument at the time of particle impact in ecliptic longitude and latitude (S_{LON} , S_{LAT}). Mean impact velocity (v , in km s^{-1}) and velocity error factor (VEF, i.e. multiply or divide stated velocity by VEF to obtain upper or lower limits) as well as mean particle mass (m , in grams) and mass error factor (MEF) are given in the last columns. For $\text{VEF} > 6$, both velocity and mass values should be discarded. This occurs for 21 impacts. No intrinsic dust charge values are given (see Svestka et al. (1996) for a detailed analysis). Recently, reliable dust charge measurements for interplanetary dust grains were reported for the Cassini dust detector. These measurements may lead to an improved understanding of the charge measurements of Ulysses and Galileo in the future.

In this paper we use different parameters to characterise particle sizes (radius, mass, impact charge, amplitude range). A conversion between these parameters is given in the appendix.

4. Analysis

The most important impact parameter determined by the dust instrument is the positive charge measured on the ion collector, Q_1 , because it is relatively insensitive to noise. Fig. 4 shows the distribution of Q_1 for all dust particles detected from 1996 to 1999. Ion impact charges have been detected over the entire range of six orders of magnitude in impact charge that can be measured by the dust instrument. The maximum measured charge was $Q_1 = 2 \times 10^{-9}$ C, well below the saturation limit of $\sim 10^{-8}$ C.

In the earlier 1993–1996 data set (Fig. 4 in Paper III) the impact charge distribution was reminiscent of three individual particle populations: small particles with impact

Table 3

Overview of dust impacts detected with the Ulysses dust detector between 1 January 1996 and 31 December 1999 as derived from the accumulators^a

Date	Time	R (AU)	Δt (d)	AC 01 ^b	AC 11 ^b	AC 21	AC 31	AC 02 ^b	AC 12	AC 22	AC 32	AC 03	AC 13	AC 23	AC 33	AC 04	AC 14	AC 24	AC 34	AC 05	AC 15	AC 25	AC 35	AC 06	AC 16	AC 26	AC 36
96-001	20:55	3.060	5.948	-	-	-	-	-	-	-	-	-	-	-	1	-	-	-	-	-	-	-	-	-	-	-	-
96-015	21:10	3.150	14.01	2	-	-	-	-	-	-	-	1	-	-	2	-	-	-	-	-	-	-	-	-	-	-	-
96-032	07:20	3.240	16.42	3	-	-	-	-	-	-	1	-	-	-	1	-	-	-	-	-	-	-	-	-	-	-	-
96-049	19:34	3.350	17.50	3	-	-	-	-	-	-	-	-	-	-	-	-	-	-	-	-	-	-	-	-	-	-	-
96-067	22:35	3.450	18.12	4	-	-	-	-	1	-	1	-	-	-	1	-	-	-	-	-	-	-	-	-	-	-	-
96-082	00:44	3.520	14.08	-	1	-	-	-	-	-	-	-	-	-	2	-	-	-	-	-	-	-	-	-	-	-	-
96-096	12:00	3.600	14.46	2	-	-	-	-	-	-	-	-	-	-	1	-	-	-	1	-	-	-	-	-	-	-	-
96-119	10:23	3.720	22.93	3	-	-	1	1	-	-	1	-	-	-	2	-	-	-	-	-	-	-	-	-	-	-	-
96-145	01:12	3.850	25.61	4	-	-	-	1	1	-	-	-	-	1	2	-	-	-	-	-	-	-	-	-	-	-	-
96-170	12:28	3.970	25.46	2	-	-	-	-	1	-	-	-	-	1	-	-	-	-	-	-	-	-	-	-	-	-	-
96-194	15:47	4.080	24.13	2	-	-	-	-	-	-	-	-	-	-	2	-	-	-	-	-	-	-	-	-	-	-	-
96-221	07:41	4.190	26.66	1	-	-	-	1	-	-	-	-	-	-	-	-	-	-	-	-	-	-	-	-	-	-	-
96-230	05:20	4.230	8.902	-	-	-	-	-	-	-	-	-	-	-	-	-	-	-	-	-	-	-	-	-	-	-	-
96-233	01:02	4.240	2.820		-----				-----				-----					-----			-----				-----		
96-254	03:25	4.320	21.09	-	1	-	-	-	-	-	-	-	-	-	-	-	-	-	-	-	-	-	-	-	-	-	-
96-281	02:43	4.420	26.97	1	-	-	-	-	-	-	-	-	-	-	-	-	-	-	1	-	-	-	-	-	-	-	-
96-305	08:51	4.510	24.25	2	-	-	-	-	-	-	-	1	-	-	-	-	-	-	-	-	-	-	-	-	-	-	-
96-320	22:16	4.570	15.55	-	-	-	-	-	-	-	2	-	1	-	1	-	-	-	-	-	-	-	-	-	-	-	-
96-359	13:34	4.690	38.63	1	-	-	-	-	-	-	1	-	-	-	-	-	-	-	1	-	-	-	-	-	-	-	-
97-015	13:30	4.760	20.99	-	-	-	-	-	-	-	-	-	1	-	1	-	-	-	-	-	-	-	-	-	-	-	-
97-028	01:22	4.790	12.49	1	-	-	-	-	-	-	-	-	-	-	-	-	-	-	-	-	-	-	-	-	-	-	-
97-060	20:57	4.880	32.81	-	-	-	-	-	-	-	1	-	-	-	1	-	-	-	-	-	-	-	-	-	-	-	-
97-091	17:50	4.960	30.87	-	-	-	-	1	1	-	-	-	-	-	-	-	-	-	-	-	-	-	-	-	-	-	-
97-093	03:29	4.960	1.402		-----				-----				-----					-----			-----				-----		
97-111	23:30	5.010	18.83	-	-	-	-	1	-	-	-	-	-	-	-	-	-	-	-	-	-	-	-	-	-	-	-
97-145	15:34	5.080	33.66	-	-	-	-	-	-	-	-	1	-	-	1	-	-	-	1	-	-	-	-	-	-	-	-
97-170	02:14	5.130	24.44	3	-	-	-	-	1	-	-	-	-	-	2	-	-	-	-	-	-	-	-	-	-	-	-
97-223	08:01	5.220	53.24	-	-	-	-	1	-	-	1	-	-	-	-	-	-	-	-	-	-	-	-	-	-	-	-
97-253	11:13	5.260	30.13	2	1	-	-	-	-	-	-	-	1	-	2	-	-	-	-	-	-	-	-	-	-	-	1
97-295	21:15	5.320	42.41	-	-	-	-	-	-	-	1	-	-	1	-	-	-	-	-	-	-	-	-	-	-	-	-
97-325	01:21	5.350	29.17	1	-	-	-	-	-	-	1	-	-	-	1	-	-	-	1	-	-	-	-	-	-	-	-
97-353	03:25	5.370	28.08	-	-	-	-	-	-	-	-	-	1	-	-	-	-	1	1	-	-	-	-	-	-	-	-
98-008	01:41	5.380	19.92	3	-	-	-	-	-	-	2	-	-	-	-	-	-	-	1	-	-	-	-	-	-	-	-
98-036	00:05	5.400	27.93	2	-	-	-	-	-	-	1	-	-	-	1	-	-	-	-	-	-	-	-	-	-	-	-
98-069	04:14	5.410	33.17	1	-	-	-	-	-	-	-	-	1	-	-	-	-	-	-	-	-	-	-	-	-	-	-
98-080	22:21	5.410	11.75	-	-	-	-	-	-	-	-	-	-	-	1	-	-	-	-	-	-	-	-	-	-	-	-
98-102	15:22	5.410	21.70	3	2	-	-	-	1	-	-	-	-	-	2	-	-	-	-	-	-	-	-	-	-	-	-
98-139	17:34	5.410	37.09	-	2	-	-	-	-	-	-	-	1	-	-	-	-	-	-	-	-	-	-	-	-	-	-

Table 3. (Continued)

Date	Time	R (AU)	Δt (d)	AC 01 ^b	AC 11 ^b	AC 21	AC 31	AC 02 ^b	AC 12	AC 22	AC 32	AC 03	AC 13	AC 23	AC 33	AC 04	AC 14	AC 24	AC 34	AC 05	AC 15	AC 25	AC 35	AC 06	AC 16	AC 26	AC 36
98-173	13:59	5.400	33.85	2	2	-	1	-	-	-	-	-	-	-	1	-	-	-	-	-	-	-	-	-	-	-	-
98-205	22:27	5.380	32.35	2	-	-	-	1	1	-	-	-	-	-	1	-	-	-	-	-	-	-	-	-	-	-	-
98-236	02:46	5.360	30.17	4	-	-	-	1	1	-	-	-	-	-	4	-	-	-	-	-	-	-	-	-	-	-	-
98-273	09:10	5.330	37.26	-	-	-	1	-	2	-	3	-	-	-	1	-	-	-	-	-	-	-	-	-	-	-	-
98-311	16:27	5.280	38.30	-	-	-	-	-	-	-	-	-	1	-	2	-	-	-	-	-	-	-	-	-	-	-	-
98-350	21:24	5.230	39.20	1	-	-	-	-	-	-	1	-	-	-	-	-	-	-	-	-	-	-	-	-	-	-	-
98-363	17:30	5.210	12.83	-	-	-	-	-	-	-	-	-	-	-	-	-	-	-	-	-	1	-	-	-	-	-	-
99-016	08:38	5.180	17.63	2	-	-	-	1	1	-	1	-	-	-	-	-	-	-	-	-	-	-	-	-	-	-	-
99-046	09:00	5.130	30.01	1	-	-	-	-	-	-	-	-	-	-	-	-	-	-	-	-	-	-	-	-	-	-	-
99-048	04:29	5.120	1.811	-	-	-	-	-	-	-	-	-	-	-	-	-	-	-	-	-	-	-	-	-	-	-	-
99-058	06:44	5.100	10.09	1	1	-	-	-	-	-	-	-	-	-	-	-	-	-	-	-	-	-	-	-	-	-	-
99-088	15:36	5.040	30.36	2	-	-	-	-	1	-	-	-	-	1	2	-	-	-	-	-	-	-	-	-	-	-	-
99-112	20:59	4.990	24.22	2	-	-	-	-	-	-	-	-	-	-	-	-	-	-	-	-	-	-	-	-	-	-	-
99-137	16:01	4.930	24.79	-	-	-	1	1	-	-	1	-	-	-	-	-	-	-	-	-	-	-	-	-	-	-	-
99-150	20:38	4.890	13.19	-	-	-	-	1	-	-	-	-	-	-	-	-	-	-	-	-	-	-	-	-	-	-	-
99-181	00:58	4.810	30.18	1	-	-	-	3	-	-	1	-	-	-	-	-	-	-	-	-	-	-	-	-	-	-	-
99-198	18:23	4.760	17.72	1	-	-	-	-	1	-	-	-	-	-	-	-	-	-	-	-	-	-	-	-	-	-	-
99-218	18:45	4.700	20.01	-	-	-	-	-	-	-	-	-	-	-	1	-	-	-	-	-	-	-	-	-	-	-	-
99-242	11:53	4.620	23.71	3	-	-	-	-	1	-	-	-	1	-	1	-	-	-	-	-	-	-	-	-	-	-	-
99-272	21:01	4.520	30.38	1	-	-	1	1	-	-	-	-	-	-	-	-	-	-	1	-	-	-	-	-	-	-	-
99-286	02:43	4.480	13.23	2	-	-	-	1	-	-	1	-	-	-	1	-	-	-	-	-	-	-	-	-	-	-	-
99-308	21:21	4.390	22.77	1	-	-	-	-	1	-	-	-	-	-	-	-	-	-	-	-	-	-	-	-	-	-	-
99-333	04:30	4.300	24.29	3	-	-	-	-	-	-	-	-	-	-	1	-	-	-	1	-	-	-	-	-	-	-	-
99-360	04:15	4.190	26.98	1	1	-	-	2	1	-	-	-	-	-	1	-	-	-	1	-	-	-	-	-	-	-	-
Impacts (counted)				-	-	0	5	-	16	0	21	2	9	4	43	0	1	1	9	0	1	0	0	0	0	0	1
Impacts (complete data)				76	11	0	5	18	16	0	21	2	9	4	43	0	1	1	9	0	1	0	0	0	0	0	1
All events (complete data)				15,295	1033	0	5	312	16	0	21	7	9	4	43	0	1	1	9	0	1	0	0	0	0	0	1

^aSwitch-on of the instrument is indicated by dashed lines. The heliocentric distance R , the lengths of the time interval Δt (days) from the previous table entry, and the corresponding numbers of impacts are given for the 24 accumulators. The accumulators are arranged with increasing signal amplitude ranges (AR), with four event classes for each amplitude range (CLN = 0, 1, 2, 3); e.g. AC31 means counter for AR = 1 and CLN = 3. The Δt in the first line (96-001) is the time interval counted from the last entry in Table 2 in Paper V. The totals of counted impacts^b, of impacts with complete data, and of all events (noise plus impact events) for the entire period are given as well.

^bEntries for AC01, AC11 and AC02 are the number of impacts with complete data. Due to the noise contamination of these three categories the number of impacts cannot be determined from the accumulators. The method to separate dust impacts from noise events in these three categories has been given by Baguhl et al. (1993).

Table 4

Raw data: No., impact time, CLN, AR, SEC, IA, EA, CA, IT, ET, EIT, EIC, ICC, PA, PET, EVD, ICP, ECP, CCP, PCP, HV and evaluated data: R , LON, LAT, D_{Jup} (in astronomical units), rotation angle (ROT), instr. pointing (S_{LON} , S_{LAT}), impact speed (V , in km s^{-1}), speed error factor (VEF), mass (m , in g) and mass error factor (MEF)

No.	Imp. Date	C	AR	S	IA	EA	CA	IT	ET	E	E	I	PA	P	E	I	E	C	P	HV	R	LON	LAT	D_{Jup}	ROT	S_{LON}	S_{LAT}	V	VEF	M	MEF
		L		E						I	I	I	E	V	V	C	C	C													
		N	C	C					T	T	C	C	T	D	P	P	P	P													
1478	96-001 20:55	3	3	167	23	27	11	8	7	6	0	1	47	0	1	0	0	0	1	3	3.05883	138.4	59.6	6.86682	114	246	-12	18.0	1.6	$7.6 \cdot 10^{-12}$	6.0
1479	96-002 16:12	0	1	208	3	7	0	9	8	9	0	0	0	0	1	0	0	0	1	3	3.06421	138.5	59.5	6.87260	171	187	-24	22.7	1.6	$7.8 \cdot 10^{-15}$	6.0
1480	96-004 12:16	0	1	186	5	10	0	7	8	8	0	0	0	0	1	0	0	0	1	3	3.07571	138.7	59.2	6.88499	136	222	-18	35.4	1.6	$4.1 \cdot 10^{-15}$	6.0
1481	96-006 11:13	3	3	199	19	24	15	6	6	6	0	1	43	0	1	0	0	0	1	3	3.08719	138.9	59.0	6.89741	153	204	-22	28.0	1.6	$3.8 \cdot 10^{-13}$	6.0
1482	96-009 04:15	0	3	220	19	22	0	7	6	6	0	0	41	0	1	0	0	0	1	3	3.10395	139.2	58.6	6.91566	177	176	-23	22.7	1.6	$5.8 \cdot 10^{-13}$	6.0
1483	96-015 21:10	3	3	177	22	28	6	6	4	5	0	1	47	0	1	0	0	0	1	3	3.14480	139.8	57.6	6.96062	103	246	-8	38.7	1.6	$4.4 \cdot 10^{-13}$	6.0
1484	96-016 15:18	0	1	155	4	8	0	10	15	0	1	0	46	31	1	0	0	0	1	3	3.14932	139.9	57.5	6.96563	72	276	1	4.9	1.7	$1.3 \cdot 10^{-12}$	7.7
1485	96-023 14:47	3	3	243	19	23	2	6	6	6	0	1	43	0	1	0	0	0	1	3	3.19043	140.5	56.6	7.01168	185	157	-22	28.0	1.6	$3.3 \cdot 10^{-13}$	6.0
1486	96-024 21:53	0	1	182	5	2	0	7	15	15	1	0	5	24	1	0	0	0	1	3	3.19860	140.7	56.4	7.02092	93	248	-5	34.1	1.9	$1.3 \cdot 10^{-15}$	10.5
1487	96-026 00:11	3	2	120	9	13	7	7	8	6	0	1	35	0	1	0	0	0	1	3	3.20527	140.7	56.3	7.02848	6	333	13	35.4	1.6	$1.3 \cdot 10^{-14}$	6.0
1488	96-032 07:20	0	1	128	6	11	0	7	7	7	0	0	6	31	1	0	0	0	1	3	3.24210	141.3	55.5	7.07058	4	329	13	43.7	1.6	$2.3 \cdot 10^{-15}$	6.0
1489	96-041 08:11	0	1	0	5	11	0	8	7	8	0	0	2	24	1	0	0	0	1	3	3.29450	142.0	54.3	7.13144	166	160	-23	34.6	1.6	$5.3 \cdot 10^{-15}$	6.0
1490	96-042 09:46	0	1	213	6	9	0	9	15	0	1	0	7	31	1	0	0	0	1	3	3.30099	142.0	54.2	7.13906	100	224	-7	5.7	2.1	$1.3 \cdot 10^{-12}$	15.7
1491	96-049 19:34	0	1	246	4	7	0	8	9	8	0	0	0	0	1	0	0	0	1	3	3.34327	142.6	53.3	7.18913	134	186	-18	25.9	1.6	$5.7 \cdot 10^{-15}$	6.0
1492	96-052 08:09	0	1	158	1	9	0	15	9	15	1	0	42	31	1	0	0	0	1	3	3.35749	142.7	53.0	7.20613	5	309	16	11.8	11.8	$7.3 \cdot 10^{-14}$	5858.3
1493	96-058 20:58	0	1	66	1	4	0	15	8	12	0	0	0	0	1	0	0	0	1	3	3.39417	143.2	52.2	7.25039	225	82	-20	11.8	11.8	$3.0 \cdot 10^{-14}$	5858.3
1494	96-062 13:19	1	2	39	9	4	5	8	12	0	1	1	0	0	1	0	0	0	1	3	3.41515	143.4	51.7	7.27596	182	127	-28	21.4	1.9	$1.6 \cdot 10^{-14}$	10.5
1495	96-064 12:54	0	1	97	2	5	0	15	10	11	0	0	0	0	1	0	0	0	1	3	3.42628	143.5	51.5	7.28961	259	46	-8	26.5	2.0	$2.7 \cdot 10^{-15}$	12.5
1496	96-064 14:18	3	2	9	14	23	8	8	7	6	0	1	42	0	1	0	0	0	1	3	3.42628	143.5	51.5	7.28961	135	177	-21	21.4	1.9	$5.8 \cdot 10^{-13}$	10.5
1497	96-067 01:32	0	1	116	6	3	0	8	15	0	1	0	35	30	1	0	0	0	1	3	3.44015	143.7	51.2	7.30667	281	25	0	21.4	1.9	$8.5 \cdot 10^{-15}$	10.5
1498	96-067 22:35	3	3	246	20	25	6	5	6	5	0	1	43	0	0	0	0	0	0	3	3.44499	143.7	51.1	7.31264	104	206	-9	35.4	1.6	$2.8 \cdot 10^{-13}$	6.0
1499	96-072 07:45	1	1	208	7	5	6	10	15	0	1	1	38	31	1	0	0	0	1	3	3.46908	144.0	50.6	7.34252	42	261	16	10.4	1.9	$1.3 \cdot 10^{-13}$	10.5
1500	96-075 23:41	3	3	254	20	25	1	6	6	6	0	1	44	0	1	0	0	0	1	3	3.48890	144.2	50.2	7.36729	103	205	-10	28.0	1.6	$5.9 \cdot 10^{-13}$	6.0
1501	96-082 00:43	3	3	29	20	25	5	5	5	5	0	1	44	0	1	0	0	0	1	3	3.52212	144.5	49.5	7.40915	139	170	-27	43.7	1.6	$1.1 \cdot 10^{-13}$	6.0
1502	96-088 06:00	3	3	242	22	28	6	7	5	6	0	1	47	0	1	0	0	0	1	3	3.55565	144.8	48.8	7.45101	72	230	5	28.1	1.6	$1.4 \cdot 10^{-12}$	6.0
1503	96-096 04:55	0	1	46	5	3	0	7	15	15	1	0	19	30	1	0	0	0	1	3	3.59739	145.2	48.0	7.50567	148	162	-34	34.1	1.9	$1.4 \cdot 10^{-15}$	10.5
1504	96-096 08:40	0	1	21	5	4	0	8	15	0	1	0	37	30	1	0	0	0	1	3	3.59804	145.2	47.9	7.50652	113	196	-16	21.4	1.9	$8.3 \cdot 10^{-15}$	10.5
1505	96-096 12:00	3	4	237	25	49	18	7	4	5	0	1	47	0	1	0	0	0	1	3	3.59870	145.2	47.9	7.50738	56	243	15	14.1	1.9	$6.5 \cdot 10^{-11}$	10.5
1506	96-102 01:33	0	1	109	5	9	0	8	7	8	0	0	5	24	1	0	0	0	1	3	3.62815	145.5	47.3	7.54578	231	61	-26	34.6	1.6	$3.8 \cdot 10^{-15}$	6.0
1507	96-103 01:35	0	2	128	9	14	0	7	7	6	0	0	37	0	1	0	0	0	1	3	3.63335	145.5	47.2	7.55261	258	38	-10	43.7	1.6	$6.4 \cdot 10^{-15}$	6.0
1508	96-103 17:53	0	1	45	7	11	0	11	15	15	1	0	99	31	1	0	0	0	1	3	3.63660	145.5	47.2	7.55687	142	169	-33	4.2	1.6	$5.7 \cdot 10^{-12}$	6.0
1509	96-105 20:51	0	1	250	4	5	0	9	15	0	1	0	17	31	1	0	0	0	1	3	3.64762	145.6	46.9	7.57137	68	233	10	14.1	1.9	$3.8 \cdot 10^{-14}$	10.5
1510	96-109 03:23	3	2	35	14	21	13	10	11	7	0	1	38	0	1	0	0	0	1	3	3.66503	145.8	46.6	7.59438	124	189	-24	10.4	1.9	$4.0 \cdot 10^{-12}$	10.5
1511	96-109 16:46	3	1	209	1	4	1	15	10	11	0	1	0	0	1	0	0	0	1	3	3.66760	145.8	46.5	7.59779	8	292	35	11.8	11.8	$3.0 \cdot 10^{-14}$	5858.3
1512	96-112 22:48	3	3	40	19	23	9	7	7	6	0	1	41	0	1	0	0	0	1	3	3.68426	145.9	46.2	7.61993	129	184	-27	21.0	1.6	$9.6 \cdot 10^{-13}$	6.0

Table 4. (Continued)

No.	Imp. Date	C L N	AR	S E C	IA	EA	CA	IT	ET	E I T	E I C	I I C	PA	P E T	E V D	I C P	E C P	C C P	P P P	HV	R	LON	LAT	D_{Jup}	ROT	S_{LON}	S_{LAT}	V	VEF	M	MEF
1513	96-119 10:23	3	3	30	22	28	13	6	5	5	0	1	47	0	1	0	0	0	1	3	3.71728	146.2	45.5	7.66416	111	201	-17	34.6	1.6	$7.0 \cdot 10^{-13}$	6.0
1514	96-125 06:28	0	1	27	4	6	0	10	15	0	1	0	22	31	1	0	0	0	1	3	3.74680	146.4	45.0	7.70406	104	208	-12	4.9	1.7	$9.0 \cdot 10^{-13}$	7.7
1515	96-125 14:27	0	1	143	1	10	0	15	9	15	1	0	43	31	1	0	0	0	1	3	3.74805	146.4	44.9	7.70576	267	33	-5	11.8	11.8	$8.6 \cdot 10^{-14}$	5858.3
1516	96-126 11:55	0	2	202	8	12	0	7	7	6	0	0	35	0	1	0	0	0	1	3	3.75242	146.5	44.8	7.71170	347	321	39	43.7	1.6	$4.0 \cdot 10^{-15}$	6.0
1517	96-130 23:59	3	3	48	21	27	3	6	5	6	0	1	46	0	1	0	0	0	1	3	3.77477	146.6	44.4	7.74219	130	189	-30	34.6	1.6	$5.0 \cdot 10^{-13}$	6.0
1518	96-133 11:14	1	2	68	14	14	7	8	8	0	1	1	39	2	1	0	0	0	1	3	3.78711	146.7	44.2	7.75912	156	161	-45	21.4	1.9	$2.0 \cdot 10^{-13}$	10.5
1519	96-135 17:11	0	1	204	3	8	0	8	7	9	0	0	0	0	1	0	0	0	1	3	3.79817	146.8	43.9	7.77433	345	326	41	34.6	1.6	$2.3 \cdot 10^{-15}$	6.0
1520	96-139 02:21	3	3	10	22	28	9	8	6	6	0	1	46	0	1	0	0	0	1	3	3.81467	146.9	43.6	7.79713	71	233	10	19.5	1.6	$5.6 \cdot 10^{-12}$	6.0
1521	96-140 06:31	2	3	57	19	23	22	6	5	6	0	1	42	0	1	0	0	0	1	3	3.82076	147.0	43.5	7.80556	138	184	-37	34.6	1.6	$1.7 \cdot 10^{-13}$	6.0
1522	96-145 01:12	0	1	231	3	8	0	8	8	10	0	0	2	24	1	0	0	0	1	3	3.84376	147.1	43.0	7.83757	19	282	41	28.0	1.6	$4.5 \cdot 10^{-15}$	6.0
1523	96-154 21:09	1	2	30	13	9	10	10	15	0	1	1	36	31	1	0	0	0	1	3	3.89094	147.5	42.1	7.90387	92	222	-4	10.4	1.9	$7.2 \cdot 10^{-13}$	10.5
1524	96-164 10:49	2	3	24	21	26	8	6	5	6	0	1	45	0	1	0	0	0	1	3	3.93553	147.8	41.3	7.96733	80	232	5	34.6	1.6	$4.2 \cdot 10^{-13}$	6.0
1525	96-169 04:12	0	1	5	4	3	0	10	15	0	1	0	39	31	1	0	0	0	1	3	3.95753	147.9	40.8	7.99892	50	254	28	10.4	1.9	$5.8 \cdot 10^{-14}$	10.5
1526	96-170 12:28	0	1	19	3	2	0	10	15	0	1	0	36	31	1	0	0	0	1	3	3.96386	148.0	40.7	8.00804	70	239	13	10.4	1.9	$4.4 \cdot 10^{-14}$	10.5
1527	96-175 20:50	0	1	139	4	5	0	7	15	0	1	0	42	31	1	0	0	0	1	3	3.98788	148.1	40.2	8.04281	236	62	-30	34.1	1.9	$1.6 \cdot 10^{-15}$	10.5
1528	96-180 21:08	0	1	58	4	1	0	9	15	0	1	0	36	31	1	0	0	0	1	3	4.01111	148.3	39.8	8.07664	118	214	-25	14.1	1.9	$2.1 \cdot 10^{-14}$	10.5
1529	96-181 18:46	3	3	49	19	23	11	6	8	6	0	1	41	0	1	0	0	0	1	3	4.01505	148.3	39.7	8.08240	106	221	-15	23.8	1.6	$5.8 \cdot 10^{-13}$	6.0
1530	96-194 15:47	3	3	53	19	25	6	5	5	6	0	1	44	0	1	0	0	0	1	3	4.07231	148.7	38.6	8.16676	104	226	-14	43.7	1.6	$8.6 \cdot 10^{-14}$	6.0
1531	96-197 08:46	0	2	164	14	22	0	8	6	6	0	0	40	0	1	0	0	0	1	3	4.08381	148.7	38.4	8.18386	258	52	-12	21.4	1.9	$5.0 \cdot 10^{-13}$	10.5
1532	96-221 07:41	0	1	59	7	11	0	7	7	7	0	0	4	24	1	0	0	0	1	3	4.18630	149.3	36.4	8.33840	86	242	1	43.7	1.6	$2.9 \cdot 10^{-15}$	6.0
1533	96-254 03:25	1	1	14	6	10	2	12	15	0	1	1	19	31	1	0	0	0	1	3	4.31903	150.1	33.9	8.54431	336	13	50	3.4	1.6	$8.0 \cdot 10^{-12}$	6.0
1534	96-261 21:47	3	4	105	24	30	18	7	4	5	0	1	47	0	1	0	0	0	1	3	4.34905	150.2	33.3	8.59178	91	249	-2	31.4	1.8	$1.8 \cdot 10^{-12}$	9.5
1535	96-281 02:43	0	1	91	1	2	0	15	15	0	1	0	2	23	1	0	0	0	1	3	4.42111	150.6	31.9	8.70704	52	274	30	11.8	11.8	$2.3 \cdot 10^{-14}$	5858.3
1536	96-289 05:04	0	1	189	3	1	0	12	15	15	1	0	42	31	1	0	0	0	1	3	4.45087	150.8	31.3	8.75516	184	150	-66	5.0	1.9	$3.3 \cdot 10^{-13}$	10.5
1537	96-292 14:17	0	1	65	3	8	0	9	8	8	0	0	0	0	1	0	0	0	1	3	4.46307	150.8	31.1	8.77499	9	325	57	22.7	1.6	$9.4 \cdot 10^{-15}$	6.0
1538	96-301 15:54	1	3	148	19	13	4	5	15	0	1	1	44	31	1	0	0	0	1	3	4.49564	151.0	30.4	8.82816	120	242	-28	34.1	1.9	$5.1 \cdot 10^{-14}$	10.5
1539	96-305 08:50	1	2	181	8	7	6	11	15	15	1	1	6	31	1	0	0	0	1	3	4.50840	151.1	30.2	8.84909	164	200	-62	7.8	1.9	$4.9 \cdot 10^{-13}$	10.5
1540	96-308 22:27	1	3	149	20	15	14	5	0	5	0	1	43	0	1	0	0	0	1	3	4.52106	151.1	29.9	8.86992	117	245	-25	34.1	1.9	$8.9 \cdot 10^{-14}$	10.5
1541	96-309 00:26	3	2	179	14	21	2	8	8	6	0	1	39	0	1	0	0	0	1	3	4.52149	151.1	29.9	8.87063	159	209	-59	21.4	1.9	$4.2 \cdot 10^{-13}$	10.5
1542	96-315 19:01	3	3	156	19	23	10	7	7	6	0	1	42	0	1	0	0	0	1	3	4.54480	151.2	29.5	8.90911	123	242	-31	21.0	1.6	$9.6 \cdot 10^{-13}$	6.0
1543	96-320 22:16	3	2	173	12	20	8	8	5	6	0	1	37	0	1	0	0	0	1	3	4.56226	151.3	29.1	8.93806	144	228	-48	21.4	1.9	$2.6 \cdot 10^{-13}$	10.5
1544	96-331 07:53	3	2	182	10	14	3	8	8	7	0	1	35	0	1	0	0	0	1	3	4.59700	151.5	28.4	8.99598	152	219	-54	28.0	1.6	$3.9 \cdot 10^{-14}$	6.0
1545	96-335 04:17	3	4	136	26	49	20	6	4	5	0	1	46	0	1	0	0	0	1	?	4.60978	151.6	28.2	9.01737	86	262	1	21.4	1.9	$1.7 \cdot 10^{-11}$	10.5
1546	96-359 13:34	0	1	151	3	1	0	8	15	0	1	0	0	0	1	0	0	0	1	3	4.68756	152.0	26.6	9.14883	94	257	-5	21.4	1.9	$3.9 \cdot 10^{-15}$	10.5
1547	97-010 02:02	1	3	65	19	13	5	6	15	15	1	1	44	31	1	0	0	0	1	3	4.73775	152.2	25.5	9.23469	322	36	40	21.4	1.9	$2.6 \cdot 10^{-13}$	10.5
1548	97-015 13:29	3	3	154	20	25	2	5	6	6	0	1	43	0	1	0	0	0	1	3	4.75405	152.3	25.2	9.26273	83	260	3	35.4	1.6	$2.8 \cdot 10^{-13}$	6.0
1549	97-028 01:22	0	1	252	3	1	0	9	15	0	1	0	0	0	1	0	0	0	1	3	4.79027	152.5	24.4	9.32537	207	108	-54	14.1	1.9	$1.8 \cdot 10^{-14}$	10.5
1550	97-043 22:37	3	3	195	21	27	6	6	5	5	0	1	46	0	1	0	0	0	1	3	4.83467	152.7	23.4	9.40269	101	245	-11	34.6	1.6	$5.0 \cdot 10^{-13}$	6.0
1551	97-060 20:57	3	2	250	12	20	10	9	9	7	0	1	38	0	1	0	0	0	1	3	4.87993	152.9	22.4	9.48209	133	223	-39	14.1	1.9	$1.2 \cdot 10^{-12}$	10.5
1552	97-068 01:39	0	2	18	9	4	0	6	15	0	1	0	22	31	1	0	0	0	1	3	4.89877	153.0	22.0	9.51530	147	210	-50	43.5	1.9	$1.2 \cdot 10^{-15}$	10.5

1553	97-080 22:16	1	2	46	13	8	9	10	15	0	1	1	4	31	1	0	0	0	1	3	4.93132	153.2	21.2	9.57292	167	179	-65	10.4	1.9	$6.0 \cdot 10^{-13}$	10.5
1554	97-111 23:30	0	2	255	12	8	0	9	15	0	1	0	19	31	1	0	0	0	1	3	5.00504	153.6	19.5	9.57292	76	242	11	14.1	1.9	$2.5 \cdot 10^{-13}$	10.5
1555	97-120 11:13	3	4	249	27	49	13	8	6	5	0	1	47	0	1	0	0	0	1	3	5.02412	153.7	19.0	9.73865	65	246	21	10.4	1.9	$1.9 \cdot 10^{-10}$	10.5
1556	97-132 16:55	0	3	48	19	14	0	8	15	0	1	0	47	31	1	0	0	0	1	3	5.05077	153.8	18.3	9.78659	138	219	-46	10.4	1.9	$2.9 \cdot 10^{-12}$	10.5
1557	97-145 15:34	3	3	19	19	22	8	6	5	6	0	1	41	0	1	0	0	0	1	3	5.07795	154.0	17.6	9.83562	94	236	-4	34.6	1.6	$1.4 \cdot 10^{-13}$	6.0
1558	97-147 15:07	0	1	246	5	4	0	10	15	0	1	0	14	30	1	0	0	0	1	3	5.08203	154.0	17.5	9.84300	54	250	33	10.4	1.9	$7.9 \cdot 10^{-14}$	10.5
1559	97-148 22:16	3	3	32	21	25	8	5	5	5	0	1	44	0	1	0	0	0	1	3	5.08457	154.0	17.4	9.84758	111	231	-20	43.7	1.6	$1.4 \cdot 10^{-13}$	6.0
1560	97-150 14:33	3	3	11	19	24	11	5	6	5	0	1	42	0	1	0	0	0	1	3	5.08785	154.0	17.3	9.85352	82	240	6	35.4	1.6	$1.8 \cdot 10^{-13}$	6.0
1561	97-155 09:59	0	1	47	7	6	0	11	15	0	1	0	25	31	1	0	0	0	1	3	5.09760	154.1	17.0	9.87115	132	225	-40	7.8	1.9	$3.4 \cdot 10^{-13}$	10.5
1562	97-166 19:46	0	1	249	7	5	0	9	10	0	1	0	46	14	1	0	0	0	1	3	5.11973	154.2	16.4	9.91123	53	251	34	14.1	1.9	$6.4 \cdot 10^{-14}$	10.5
1563	97-170 02:14	1	2	79	9	3	5	9	15	0	1	1	13	31	1	0	0	0	1	3	5.12590	154.3	16.2	9.92241	173	182	-77	14.1	1.9	$6.6 \cdot 10^{-14}$	10.5
1564	97-183 13:43	3	2	11	14	21	8	7	7	6	0	1	40	0	1	0	0	0	1	3	5.15079	154.4	15.5	9.96754	75	244	14	34.1	1.9	$8.3 \cdot 10^{-14}$	10.5
1565	97-223 08:01	0	2	87	10	5	0	9	15	0	1	0	41	31	1	0	0	0	1	3	5.21721	154.8	13.4	10.08808	156	229	-64	14.1	1.9	$1.1 \cdot 10^{-13}$	10.5
1566	97-228 12:46	3	3	33	19	24	25	5	6	6	0	1	43	0	1	0	0	0	1	3	5.22522	154.9	13.2	10.10260	69	252	19	35.4	1.6	$1.8 \cdot 10^{-13}$	6.0
1567	97-231 15:51	1	3	64	19	22	13	6	6	0	1	1	99	16	1	0	0	0	1	3	5.22991	154.9	13.0	10.11109	104	246	-14	28.0	1.6	$2.8 \cdot 10^{-13}$	6.0
1568	97-236 04:53	0	1	48	1	1	0	15	0	11	0	0	10	23	1	0	0	0	1	3	5.23655	155.0	12.8	10.12310	74	252	15	11.8	11.8	$1.9 \cdot 10^{-14}$	5858.3
1569	97-237 07:43	3	6	249	57	49	13	8	6	5	0	1	47	0	1	1	0	0	1	3	5.23819	155.0	12.7	10.12607	344	22	67	10.4	1.9	$1.6 \cdot 10^{-09}$	10.5
1570	97-238 10:04	3	3	78	19	23	5	7	7	6	0	1	41	0	1	0	0	0	1	3	5.23982	155.0	12.6	10.12902	104	247	-13	21.0	1.6	$9.6 \cdot 10^{-13}$	6.0
1571	97-247 23:29	0	1	92	3	2	0	8	15	0	1	0	0	0	1	0	0	0	1	3	5.25328	155.1	12.2	10.15334	81	253	8	21.4	1.9	$4.6 \cdot 10^{-15}$	10.5
1572	97-253 11:13	1	1	96	3	4	2	10	15	0	1	1	7	31	1	0	0	0	1	3	5.26081	155.2	11.9	10.16692	72	255	17	10.4	1.9	$5.7 \cdot 10^{-14}$	10.5
1573	97-274 21:29	2	3	140	20	25	24	5	5	5	0	1	44	0	1	0	0	0	1	3	5.28842	155.4	10.8	10.21649	105	253	-15	43.7	1.6	$1.1 \cdot 10^{-13}$	6.0
1574	97-295 21:15	3	2	154	8	13	2	7	8	7	0	1	34	0	1	0	0	0	1	3	5.31259	155.6	9.7	10.25945	116	255	-25	35.4	1.6	$1.1 \cdot 10^{-14}$	6.0
1575	97-300 08:40	3	4	1	28	49	28	12	10	8	0	1	15	0	1	0	0	0	1	3	5.31728	155.6	9.5	10.26772	260	70	-10	2.0	1.9	$5.1 \cdot 10^{-08}$	10.5
1576	97-308 20:54	3	3	170	19	22	4	8	6	6	0	1	41	0	1	0	0	0	1	3	5.32604	155.7	9.1	10.28311	136	254	-45	19.5	1.6	$1.1 \cdot 10^{-12}$	6.0
1577	97-313 18:51	0	1	189	2	2	0	15	9	0	1	0	99	27	1	0	0	0	1	3	5.33099	155.8	8.8	10.29175	161	246	-70	11.8	11.8	$2.8 \cdot 10^{-14}$	5858.3
1578	97-325 01:21	3	2	144	11	19	6	9	7	7	0	1	36	0	1	0	0	0	1	3	5.34155	155.9	8.3	10.31004	97	260	-6	14.1	1.9	$7.7 \cdot 10^{-13}$	10.5
1579	97-329 04:12	2	4	162	29	49	17	7	9	5	0	1	46	0	1	0	0	0	1	3	5.34523	155.9	8.1	10.31636	121	257	-30	14.1	1.9	$1.2 \cdot 10^{-10}$	10.5
1580	97-343 12:22	1	3	134	19	12	8	7	15	0	1	1	9	31	1	0	0	0	1	3	5.35722	156.0	7.3	10.33670	80	263	9	14.1	1.9	$1.0 \cdot 10^{-12}$	10.5
1581	97-353 03:25	1	4	178	28	8	17	7	15	4	1	1	99	1	1	0	0	0	1	3	5.36454	156.1	6.9	10.34888	139	256	-48	14.1	1.9	$2.5 \cdot 10^{-12}$	10.5
1582	97-355 05:19	0	1	114	4	3	0	7	7	11	0	0	12	23	1	0	0	0	1	3	5.36599	156.2	6.8	10.35127	51	268	38	34.1	1.9	$1.2 \cdot 10^{-15}$	10.5
1583	97-358 10:24	0	1	188	2	3	0	11	11	6	0	0	4	13	1	0	0	0	1	3	5.36829	156.2	6.6	10.35503	154	253	-63	11.8	11.8	$3.2 \cdot 10^{-14}$	5858.3
1584	97-358 14:00	0	1	206	6	10	0	8	8	9	0	0	0	0	1	0	0	0	1	3	5.36838	156.2	6.6	10.35518	179	190	-87	28.0	1.6	$1.0 \cdot 10^{-14}$	6.0
1585	97-359 02:25	3	4	68	29	49	20	9	7	5	0	1	1	0	1	0	0	0	1	3	5.36872	156.2	6.6	10.35574	345	38	71	7.8	1.9	$5.4 \cdot 10^{-10}$	10.5
1586	97-361 19:23	3	2	141	9	14	4	9	9	9	0	1	36	0	1	0	0	0	1	3	5.37061	156.2	6.4	10.35881	87	262	3	21.0	1.6	$9.8 \cdot 10^{-14}$	6.0
1587	98-008 01:41	3	2	164	11	20	7	8	6	6	0	1	37	0	1	0	0	0	1	3	5.37784	156.3	5.9	10.37035	118	257	-27	21.4	1.9	$2.2 \cdot 10^{-13}$	10.5
1588	98-022 16:15	3	2	175	11	20	3	7	5	7	0	1	37	0	1	0	0	0	1	3	5.38608	156.5	5.2	10.38297	130	255	-39	34.1	1.9	$4.4 \cdot 10^{-14}$	10.5
1589	98-025 12:28	0	1	118	1	4	0	15	4	0	1	0	0	0	1	0	0	0	1	3	5.38755	156.5	5.0	10.38513	49	264	39	11.8	11.8	$3.0 \cdot 10^{-14}$	5858.3
1590	98-029 12:06	3	3	129	19	24	8	5	6	6	0	1	43	0	1	0	0	0	1	3	5.38950	156.5	4.8	10.38797	64	261	25	35.4	1.6	$1.8 \cdot 10^{-13}$	6.0
1591	98-036 00:05	0	1	211	3	4	0	11	14	0	1	0	3	23	1	0	0	0	1	3	5.39247	156.6	4.5	10.39215	176	245	-85	7.8	1.9	$1.2 \cdot 10^{-13}$	10.5
1592	98-039 10:16	1	3	129	20	21	4	4	14	0	1	1	46	31	1	0	0	0	1	3	5.39391	156.6	4.4	10.39410	59	259	30	43.5	1.9	$6.3 \cdot 10^{-14}$	10.5
1593	98-069 04:13	0	1	189	1	3	0	15	13	11	0	0	11	23	1	0	0	0	1	3	5.40358	156.9	2.9	10.40511	350	25	77	11.8	11.8	$2.6 \cdot 10^{-14}$	5858.3
1594	98-080 22:21	3	3	20	21	26	28	5	5	5	0	1	45	0	1	0	0	0	1	3	5.40591	157.0	2.3	10.40636	106	247	-15	43.7	1.6	$1.6 \cdot 10^{-13}$	6.0
1595	98-083 23:56	3	3	20	23	29	4	3	3	5	0	1	46	0	1	0	0	0	1	3	5.40638	157.0	2.2	10.40640	104	246	-13	70.0	1.6	$5.5 \cdot 10^{-14}$	6.0
1596	98-088 22:15	0	1	50	7	11	0	9	9	8	0	0	0	0	1	0	0	0	1	3	5.40702	157.1	2.0	10.40620	145	246	-54	21.0	1.6	$4.4 \cdot 10^{-14}$	6.0
1597	98-091 16:54	0	1	86	2	6	0	9	8	9	0	0	6	31	1	0	0	0	1	3	5.40731	157.1	1.8	10.40596	194	48	-74	36.7	2.0	$1.1 \cdot 10^{-15}$	12.5

Table 4. (Continued)

No.	Imp. Date	C L N	AR	S E C	IA	EA	CA	IT	ET	E I T	E I C	I I C	PA	P E T	E V D	I V P	E C P	C C P	P P P	HV	R	LON	LAT	D_{Jup}	ROT	S_{LON}	S_{LAT}	V	VEF	M	MEF
1598	98-094 03:55	1	2	46	12	12	8	8	8	0	1	1	0	0	1	0	0	0	1	3	5.40753	157.1	1.7	10.40566	137	245	-46	21.4	1.9	$1.1 \cdot 10^{-13}$	10.5
1599	98-095 06:47	0	1	248	3	4	0	10	15	0	1	0	39	31	1	0	0	0	1	3	5.40762	157.1	1.6	10.40550	61	246	28	10.4	1.9	$5.7 \cdot 10^{-14}$	10.5
1600	98-097 22:11	3	3	27	20	24	17	5	6	6	0	1	42	0	1	0	0	0	1	3	5.40780	157.2	1.5	10.40506	112	244	-21	35.4	1.6	$2.4 \cdot 10^{-13}$	6.0
1601	98-099 06:11	1	1	241	4	5	2	12	15	0	1	1	11	31	1	0	0	0	1	3	5.40787	157.2	1.5	10.40479	50	247	40	5.0	1.9	$7.0 \cdot 10^{-13}$	10.5
1602	98-102 15:22	1	1	70	1	2	1	15	15	0	1	1	3	20	1	0	0	0	1	3	5.40801	157.2	1.3	10.40403	171	260	-79	11.8	11.8	$2.3 \cdot 10^{-14}$	5858.3
1603	98-139 06:14	1	1	37	3	5	5	14	13	0	1	1	0	0	1	0	0	0	1	3	5.40503	157.6	-0.5	10.38651	122	243	-31	3.9	1.6	$1.3 \cdot 10^{-12}$	6.0
1604	98-139 14:44	1	1	3	4	3	4	10	15	0	1	1	9	31	1	0	0	0	1	3	5.40498	157.6	-0.5	10.38633	74	242	16	10.4	1.9	$5.8 \cdot 10^{-14}$	10.5
1605	98-139 17:34	1	3	5	19	20	3	8	7	0	1	1	21	4	1	0	0	0	1	3	5.40495	157.6	-0.5	10.38624	77	242	13	10.4	1.9	$5.3 \cdot 10^{-12}$	10.5
1606	98-145 13:37	0	1	159	6	11	0	7	7	8	0	0	0	0	1	0	0	0	1	3	5.40370	157.6	-0.8	10.38182	295	51	25	43.7	1.6	$2.3 \cdot 10^{-15}$	6.0
1607	98-147 20:24	1	1	249	3	4	2	11	13	0	1	1	9	31	1	0	0	0	1	3	5.40316	157.6	-0.9	10.38000	60	242	30	7.8	1.9	$1.2 \cdot 10^{-13}$	10.5
1608	98-153 11:54	1	1	18	7	5	5	12	15	0	1	1	11	31	1	0	0	0	1	3	5.40169	157.7	-1.2	10.37519	97	242	-6	5.0	1.9	$1.2 \cdot 10^{-12}$	10.5
1609	98-161 07:21	3	3	18	19	24	11	6	6	5	0	1	42	0	1	0	0	0	1	3	5.39930	157.8	-1.6	10.36778	97	243	-6	28.0	1.6	$3.8 \cdot 10^{-13}$	6.0
1610	98-162 23:44	0	1	10	6	19	0	10	4	8	0	0	39	0	1	0	0	0	1	3	5.39877	157.8	-1.6	10.36615	85	243	5	10.4	1.9	$7.0 \cdot 10^{-13}$	10.5
1611	98-173 13:59	3	1	12	7	11	4	7	7	6	0	1	0	0	1	0	0	0	1	3	5.39484	157.9	-2.2	10.35469	89	244	1	43.7	1.6	$2.9 \cdot 10^{-15}$	6.0
1612	98-182 19:15	0	1	152	4	1	0	8	15	0	1	0	5	23	1	0	0	0	1	3	5.39086	158.0	-2.6	10.34354	287	55	17	21.4	1.9	$4.5 \cdot 10^{-15}$	10.5
1613	98-200 16:10	0	2	132	9	15	0	7	8	6	0	0	36	0	1	0	0	0	1	3	5.38168	158.1	-3.5	10.31893	261	56	-8	34.1	1.9	$2.0 \cdot 10^{-14}$	10.5
1614	98-201 23:14	0	1	21	4	19	0	10	6	13	0	0	36	0	1	0	0	0	1	3	5.38097	158.1	-3.5	10.31705	105	248	-14	10.4	1.9	$5.0 \cdot 10^{-13}$	10.5
1615	98-202 13:44	1	2	231	11	13	6	9	15	0	1	1	24	31	1	0	0	0	1	3	5.38061	158.1	-3.6	10.31611	41	246	49	5.7	2.1	$5.8 \cdot 10^{-12}$	15.7
1616	98-205 22:27	3	3	242	19	23	3	6	7	6	0	1	41	0	1	0	0	0	1	3	5.37862	158.2	-3.7	10.31093	57	246	33	25.9	1.6	$4.3 \cdot 10^{-13}$	6.0
1617	98-207 01:42	0	2	252	10	14	0	7	8	6	0	0	35	0	1	0	0	0	1	3	5.37794	158.2	-3.8	10.30917	71	247	20	35.4	1.6	$1.8 \cdot 10^{-14}$	6.0
1618	98-210 03:24	0	1	46	6	10	0	8	8	9	0	0	4	31	1	0	0	0	1	3	5.37601	158.2	-3.9	10.30420	143	255	-51	28.0	1.6	$1.0 \cdot 10^{-14}$	6.0
1619	98-214 02:36	3	3	253	19	22	14	10	11	7	0	1	37	0	1	0	0	0	1	3	5.37354	158.3	-4.1	10.29787	75	248	16	6.2	1.6	$3.2 \cdot 10^{-11}$	6.0
1620	98-220 18:13	3	3	8	20	25	4	5	6	5	0	1	44	0	1	0	0	0	1	3	5.36901	158.3	-4.5	10.28639	93	250	-2	35.4	1.6	$2.8 \cdot 10^{-13}$	6.0
1621	98-222 10:05	3	3	251	19	25	6	6	7	5	0	1	43	0	1	0	0	0	1	3	5.36788	158.3	-4.5	10.28354	76	249	14	25.9	1.6	$5.9 \cdot 10^{-13}$	6.0
1622	98-224 20:40	0	1	20	2	9	0	15	15	0	1	0	99	31	1	0	0	0	1	3	5.36619	158.4	-4.7	10.27932	111	252	-19	11.8	11.8	$8.8 \cdot 10^{-14}$	5858.3
1623	98-232 21:14	3	3	36	20	25	1	5	5	6	0	1	45	0	1	0	0	0	1	3	5.36017	158.4	-5.1	10.26433	146	262	-54	43.7	1.6	$1.1 \cdot 10^{-13}$	6.0
1624	98-233 11:26	0	1	239	7	8	0	13	10	0	1	0	99	22	1	0	0	0	1	3	5.35979	158.4	-5.1	10.26338	73	251	18	2.5	1.9	$2.1 \cdot 10^{-11}$	10.5
1625	98-233 18:56	0	1	220	2	1	0	11	15	14	0	0	99	4	1	0	0	0	1	3	5.35950	158.4	-5.1	10.26267	46	250	44	11.8	11.8	$2.4 \cdot 10^{-14}$	5858.3
1626	98-236 02:46	1	2	15	8	12	8	12	15	0	1	1	20	31	1	0	0	0	1	3	5.35775	158.5	-5.2	10.25834	124	256	-32	3.4	1.6	$1.6 \cdot 10^{-11}$	6.0
1627	98-239 17:56	3	2	229	14	22	13	9	9	7	0	1	40	0	1	0	0	0	1	3	5.35486	158.5	-5.4	10.25125	90	253	1	14.1	1.9	$2.3 \cdot 10^{-12}$	10.5
1628	98-241 07:52	3	2	244	9	14	2	9	9	8	0	1	0	0	1	0	0	0	1	3	5.35354	158.5	-5.5	10.24802	126	257	-34	21.0	1.6	$9.8 \cdot 10^{-14}$	6.0
1629	98-249 22:07	1	2	200	13	10	10	8	9	0	1	1	0	0	1	0	0	0	1	3	5.34625	158.6	-5.9	10.23030	121	258	-29	21.4	1.9	$9.0 \cdot 10^{-14}$	10.5
1630	98-251 04:52	1	2	180	12	5	6	8	15	0	1	1	0	0	1	0	0	0	1	3	5.34516	158.6	-6.0	10.22765	97	255	-6	21.4	1.9	$3.1 \cdot 10^{-14}$	10.5
1631	98-254 22:37	3	3	151	21	26	10	5	6	5	0	1	44	0	1	0	0	0	1	3	5.34182	158.6	-6.2	10.21960	68	253	23	35.4	1.6	$3.9 \cdot 10^{-13}$	6.0
1632	98-262 10:12	3	1	160	7	11	1	8	8	7	0	1	2	23	1	0	0	0	1	3	5.33488	158.7	-6.5	10.20298	96	257	-4	28.0	1.6	$1.5 \cdot 10^{-14}$	6.0
1633	98-273 09:10	3	2	143	14	21	8	8	7	6	0	1	40	0	1	0	0	0	1	3	5.32406	158.8	-7.1	10.17733	77	257	14	21.4	1.9	$4.2 \cdot 10^{-13}$	10.5
1634	98-283 05:38	1	3	229	18	11	13	12	15	0	1	1	99	31	1	0	0	0	1	3	5.31385	158.9	-7.6	10.15335	203	49	-63	2.0	1.9	$3.3 \cdot 10^{-10}$	10.5
1635	98-287 03:20	3	3	155	20	24	20	5	5	5	0	1	43	0	1	0	0	0	1	3	5.30949	159.0	-7.8	10.14317	100	262	-8	43.7	1.6	$9.8 \cdot 10^{-14}$	6.0
1636	98-311 16:27	3	3	148	19	22	10	9	9	6	0	1	39	0	1	0	0	0	1	3	5.28059	159.2	-9.0	10.07655	93	263	-1	12.6	1.6	$4.7 \cdot 10^{-12}$	6.0
1637	98-319 10:27	3	2	125	13	20	5	9	7	8	0	1	38	0	1	0	0	0	1	3	5.27067	159.3	-9.4	10.05396	62	260	28	14.1	1.9	$1.4 \cdot 10^{-12}$	10.5

1638	98-350 21:24	0	1	143	1	8	0	15	7	12	0	0	0	0	1	0	0	0	1	3	5.22641	159.6	-11.0	9.95466	91	266	0	11.8	11.8	$6.1 \cdot 10^{-14}$	5858.3
1639	98-363 17:29	1	5	163	55	56	30	14	12	0	1	1	33	31	1	0	0	0	1	3	5.20671	159.7	-11.7	9.91111	125	275	-31	2.0	1.9	$8.2 \cdot 10^{-07}$	10.5
1640	99-007 22:18	0	2	168	8	7	0	9	15	0	1	0	10	31	1	0	0	0	1	3	5.19176	159.8	-12.2	9.87831	135	279	-40	14.1	1.9	$1.1 \cdot 10^{-13}$	10.5
1641	99-008 15:37	0	1	85	5	9	0	11	15	0	1	0	19	31	1	0	0	0	1	3	5.19053	159.8	-12.2	9.87561	18	235	71	4.2	1.6	$2.8 \cdot 10^{-12}$	6.0
1642	99-013 00:20	0	1	147	2	3	0	10	15	0	1	0	1	31	1	0	0	0	1	3	5.18324	159.9	-12.4	9.85971	106	268	-13	11.8	11.8	$3.2 \cdot 10^{-14}$	5858.3
1643	99-013 06:04	3	2	129	15	22	2	8	7	6	0	1	41	0	1	0	0	0	1	3	5.18282	159.9	-12.5	9.85879	81	262	10	21.4	1.9	$5.4 \cdot 10^{-13}$	10.5
1644	99-016 08:38	1	2	48	12	10	6	9	15	0	1	1	40	31	1	0	0	0	1	3	5.17775	159.9	-12.6	9.84775	329	93	58	14.1	1.9	$3.5 \cdot 10^{-13}$	10.5
1645	99-040 14:08	0	1	114	3	7	0	8	8	9	0	0	0	0	1	0	0	0	1	3	5.13463	160.2	-13.9	9.75469	82	258	9	28.0	1.6	$3.7 \cdot 10^{-15}$	6.0
1646	99-052 07:32	1	1	63	5	2	2	9	15	0	1	1	12	31	1	0	0	0	1	3	5.11236	160.3	-14.5	9.70717	36	237	52	14.1	1.9	$2.9 \cdot 10^{-14}$	10.5
1647	99-058 06:44	0	1	246	2	1	0	15	15	0	1	0	36	31	1	0	0	0	1	3	5.10064	160.4	-14.9	9.68230	314	82	43	11.8	11.8	$2.4 \cdot 10^{-14}$	5858.3
1648	99-059 11:10	2	3	94	21	26	13	9	8	6	0	1	45	0	1	0	0	0	1	3	5.09842	160.4	-14.9	9.67760	108	261	-14	14.4	1.6	$9.9 \cdot 10^{-12}$	6.0
1649	99-080 14:23	3	3	31	23	29	26	7	5	5	0	1	47	0	1	0	0	0	1	3	5.05510	160.6	-16.1	9.58659	79	247	12	28.1	1.6	$1.9 \cdot 10^{-12}$	6.0
1650	99-081 21:16	1	2	41	11	8	9	9	15	0	1	1	4	23	1	0	0	0	1	3	5.05218	160.6	-16.2	9.58049	94	252	-1	14.1	1.9	$2.1 \cdot 10^{-13}$	10.5
1651	99-082 04:35	0	1	218	1	4	0	15	0	13	0	0	0	0	1	0	0	0	1	3	5.05165	160.6	-16.2	9.57938	343	105	68	11.8	11.8	$3.0 \cdot 10^{-14}$	5858.3
1652	99-088 03:51	0	1	73	6	11	0	7	8	6	0	0	0	0	1	0	0	0	1	3	5.03874	160.7	-16.5	9.55253	146	278	-48	35.4	1.6	$5.7 \cdot 10^{-15}$	6.0
1653	99-088 15:36	3	3	93	21	26	3	5	5	5	0	1	46	0	1	0	0	0	1	3	5.03765	160.7	-16.5	9.55027	175	322	-64	43.7	1.6	$1.6 \cdot 10^{-13}$	6.0
1654	99-094 09:48	0	1	63	6	10	0	7	7	7	0	0	0	0	1	0	0	0	1	3	5.02504	160.8	-16.9	9.52414	138	270	-41	43.7	1.6	$2.0 \cdot 10^{-15}$	6.0
1655	99-104 17:43	0	1	245	2	2	0	15	15	0	1	0	8	31	1	0	0	0	1	3	5.00200	160.9	-17.4	9.47667	41	226	48	11.8	11.8	$2.8 \cdot 10^{-14}$	5858.3
1656	99-112 20:59	3	2	22	12	20	2	8	6	7	0	1	37	0	1	0	0	0	1	3	4.98323	161.0	-17.9	9.43825	91	245	1	21.4	1.9	$2.6 \cdot 10^{-13}$	10.5
1657	99-115 05:54	0	2	197	8	1	0	5	15	11	0	0	4	22	1	0	0	0	1	3	4.97766	161.0	-18.0	9.42689	338	93	64	70.0	1.9	$9.6 \cdot 10^{-17}$	10.5
1658	99-137 16:00	3	1	156	7	12	5	7	7	6	0	1	0	0	1	0	0	0	1	3	4.92299	161.3	-19.3	9.31633	289	61	20	43.7	1.6	$3.3 \cdot 10^{-15}$	6.0
1659	99-150 20:38	0	2	10	9	19	0	9	8	9	0	0	37	0	1	0	0	0	1	3	4.88949	161.5	-20.1	9.24944	88	243	4	14.1	1.9	$5.7 \cdot 10^{-13}$	10.5
1660	99-152 12:17	0	1	94	5	6	0	8	15	0	1	0	39	31	1	0	0	0	1	3	4.88494	161.5	-20.2	9.24039	206	18	-53	21.4	1.9	$1.2 \cdot 10^{-14}$	10.5
1661	99-157 13:23	0	2	20	10	14	0	8	8	6	0	0	35	0	1	0	0	0	1	3	4.87180	161.6	-20.5	9.21437	105	249	-11	28.0	1.6	$3.9 \cdot 10^{-14}$	6.0
1662	99-165 01:16	3	2	32	13	21	14	7	5	6	0	1	39	0	1	0	0	0	1	3	4.85177	161.7	-21.0	9.17487	124	258	-29	34.1	1.9	$7.1 \cdot 10^{-14}$	10.5
1663	99-179 00:37	0	2	94	8	8	0	14	15	0	1	0	41	27	1	0	0	0	1	3	4.81332	161.9	-21.8	9.09970	216	30	-46	2.0	1.9	$6.4 \cdot 10^{-11}$	10.5
1664	99-181 00:58	0	2	74	8	13	0	8	8	7	0	0	35	0	1	0	0	0	1	3	4.80772	161.9	-21.9	9.08880	189	351	-63	28.0	1.6	$2.4 \cdot 10^{-14}$	6.0
1665	99-196 11:11	1	2	255	14	22	4	13	12	0	1	1	31	31	1	0	0	0	1	3	4.76368	162.1	-22.9	9.00382	91	249	1	2.5	1.9	$4.3 \cdot 10^{-10}$	10.5
1666	99-198 18:22	0	1	17	3	8	0	8	8	9	0	0	0	0	1	0	0	0	1	3	4.75673	162.1	-23.0	8.99049	117	259	-22	28.0	1.6	$4.5 \cdot 10^{-15}$	6.0
1667	99-218 18:45	3	3	246	19	23	8	9	9	6	0	1	40	0	1	0	0	0	1	3	4.69656	162.4	-24.3	8.87630	95	253	-2	12.6	1.6	$5.4 \cdot 10^{-12}$	6.0
1668	99-222 09:16	0	1	199	5	10	0	7	7	8	0	0	10	23	1	0	0	0	1	3	4.68535	162.5	-24.5	8.85522	33	226	54	43.7	1.6	$1.7 \cdot 10^{-15}$	6.0
1669	99-223 00:23	0	1	238	4	2	0	9	15	0	1	0	34	31	1	0	0	0	1	3	4.68341	162.5	-24.6	8.85158	88	252	4	14.1	1.9	$2.5 \cdot 10^{-14}$	10.5
1670	99-225 21:14	1	3	207	20	8	11	7	15	0	1	1	45	31	1	0	0	0	1	?	4.67443	162.5	-24.7	8.83477	49	237	40	14.1	1.9	$7.0 \cdot 10^{-13}$	10.5
1671	99-227 07:11	1	2	249	12	22	9	10	14	0	1	1	25	31	1	0	0	0	1	3	4.67012	162.6	-24.8	8.82670	111	261	-17	10.4	1.9	$3.4 \cdot 10^{-12}$	10.5
1672	99-235 16:00	3	3	21	23	28	5	6	4	5	0	1	46	0	1	0	0	0	1	3	4.64354	162.7	-25.4	8.77724	161	302	-57	38.7	1.6	$5.2 \cdot 10^{-13}$	6.0
1673	99-242 11:53	0	1	207	2	1	0	15	15	0	1	0	0	0	1	0	0	0	1	3	4.62174	162.8	-25.8	8.73695	80	253	11	11.8	11.8	$2.4 \cdot 10^{-14}$	5858.3
1674	99-257 06:03	0	1	231	2	2	0	15	15	0	1	0	4	23	1	0	0	0	1	3	4.57252	163.0	-26.8	8.64687	144	288	-45	11.8	11.8	$2.8 \cdot 10^{-14}$	5858.3
1675	99-270 12:05	3	1	157	4	9	13	7	7	7	0	1	0	0	1	0	0	0	1	3	4.52727	163.2	-27.7	8.56519	58	249	31	43.7	1.6	$1.2 \cdot 10^{-15}$	6.0
1676	99-272 03:19	0	2	159	14	21	0	8	5	7	0	0	43	0	1	0	0	0	1	3	4.52163	163.3	-27.8	8.55508	65	252	25	21.4	1.9	$4.2 \cdot 10^{-13}$	10.5
1677	99-272 21:01	3	4	220	27	49	11	8	6	5	0	1	46	0	1	0	0	0	1	3	4.51902	163.3	-27.9	8.55041	150	298	-49	10.4	1.9	$1.9 \cdot 10^{-10}$	10.5
1678	99-273 11:55	3	2	13	10	14	17	7	8	6	0	1	36	0	1	0	0	0	1	3	4.51727	163.3	-27.9	8.54730	219	46	-42	35.4	1.6	$1.8 \cdot 10^{-14}$	6.0
1679	99-278 10:02	0	2	115	10	2	0	9	15	0	1	0	37	31	1	0	0	0	1	3	4.49975	163.4	-28.3	8.51603	10	197	69	14.1	1.9	$6.8 \cdot 10^{-14}$	10.5
1680	99-280 03:07	3	3	125	23	30	8	8	4	5	0	1	46	0	1	0	0	0	1	3	4.49357	163.4	-28.4	8.50504	23	222	61	10.4	1.9	$5.8 \cdot 10^{-11}$	10.5
1681	99-282 09:17	0	1	198	5	9	0	8	8	8	0	0	9	31	1	0	0	0	1	3	4.48559	163.5	-28.5	8.49089	129	283	-31	28.0	1.6	$7.4 \cdot 10^{-15}$	6.0
1682	99-286 02:42	0	1	239	6	10	0	8	8	7	0	0	0	0	1	0	0	0	1	3	4.47265	163.5	-28.8	8.46800	189	7	-59	28.0	1.6	$1.0 \cdot 10^{-14}$	6.0

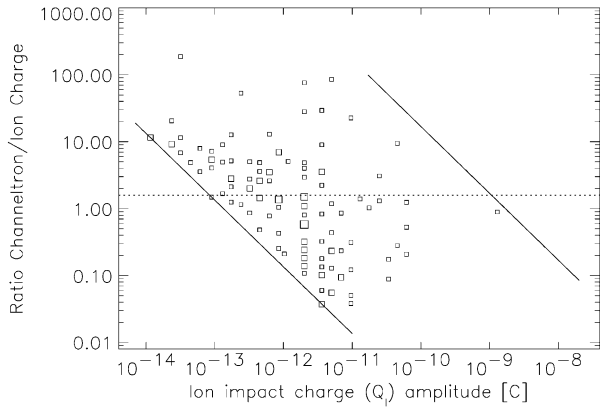


Fig. 5. Channeltron amplification factor $A = Q_C/Q_I$ as a function of impact charge Q_I for all dust impacts detected between 1996 and 1999. The solid lines denote the sensitivity threshold (lower left) and the saturation limit (upper right) of the channeltron. Squares indicate dust particle impacts. The area of each square is proportional to the number of events included (the scaling of the squares is the same as that in Paper III). The dotted horizontal line shows the mean value of the channeltron amplification $A = 1.6$ for ion impact charges $10^{-12} \text{ C} < Q_I < 10^{-11} \text{ C}$.

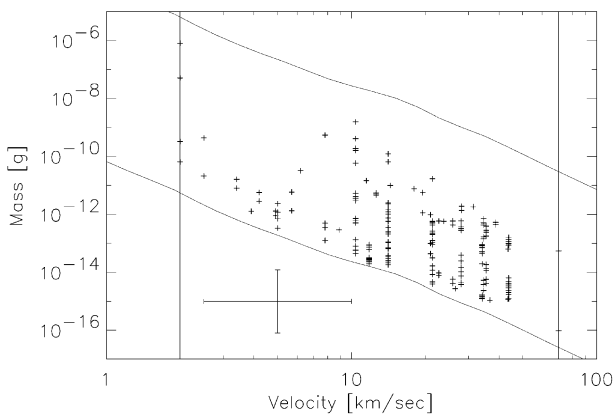


Fig. 6. Masses and impact velocities of all impacts recorded with the Ulysses sensor from 1996 to 1999. The lower and upper solid lines indicate the threshold and the saturation limit of the detector, respectively, and the vertical lines indicate the calibrated velocity range. A sample error bar is shown that indicates a factor of 2 uncertainty for the velocity and a factor of 10 for the mass determination.

radiation environment in the magnetosphere of the giant planet. The channeltron high voltage of the Ulysses detector will have to be increased in the future, as has already been done with the Galileo detector. The channeltron degradation is the reason that not all noise tests show up as individual sharp spikes in Fig. 3.

In Fig. 6, we show the masses and velocities of all dust particles detected between 1996 and 1999. As in the earlier period (1990–1995, Papers III and V) velocities occur over the entire calibrated range from 2 to 70 km s^{-1} . The masses vary over 10 orders of magnitude from 10^{-6} to 10^{-16} g. The mean errors are a factor of 2 for the velocity and a factor of 10 for the mass. The clustering of the velocity values is due to discrete steps in the rise time measurement but this quan-

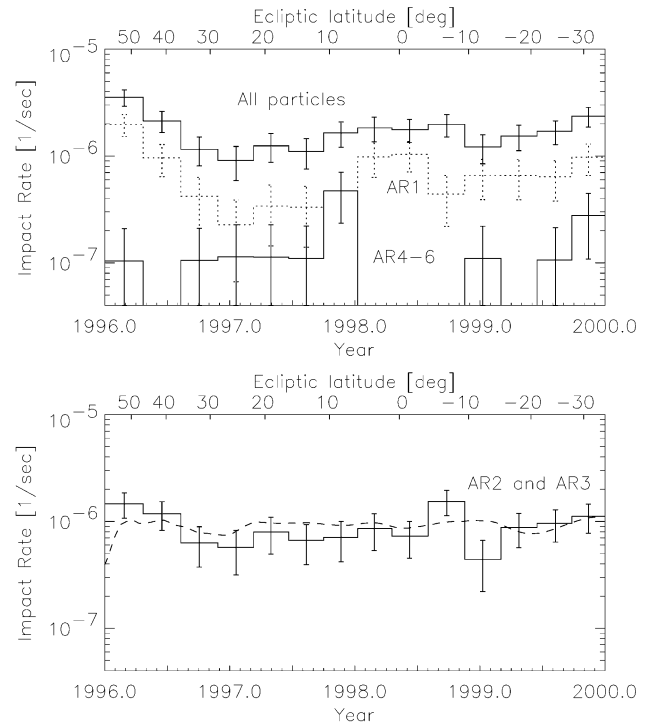


Fig. 7. Impact rate of dust particles detected with the Ulysses dust sensor as a function of time. The ecliptic latitude of the spacecraft is indicated at the top. Upper panel: total impact rate (upper solid histograms), impact rate of small particles (AR1, dotted histograms), and impact rate of big particles (AR4–AR6, lower solid histograms). Note that a rate of about 1.0×10^{-7} impacts/s is caused by a single dust impact in the averaging interval of about 110 days. Lower panel: impact rate of intermediate size particles (AR2 and AR3, solid histograms). A model for the rate of interstellar particles assuming a constant flux is superimposed as a dashed line. Vertical bars indicate the \sqrt{n} statistical error.

tisation is much smaller than the velocity uncertainty. For many particles in the lowest two amplitude ranges (AR1 and AR2) the velocity had to be computed from the ion charge signal alone which leads to the striping in the lower mass range in Fig. 6 (most prominent above 10 km s^{-1}). In the higher amplitude ranges the velocity could normally be calculated from both the target and the ion charge signal, resulting in a more continuous distribution in the mass–velocity plane. Impact velocities below about 3 km s^{-1} should be treated with caution because anomalous impacts onto the sensor grids or structures other than the target generally lead to prolonged rise times and hence to unnaturally low impact velocities.

5. Discussion

In the time period considered in this paper the Ulysses spacecraft was beyond 3 AU from the Sun and at relatively low ecliptic latitudes most of the time ($\beta \leq 30^\circ$ after 1996). Fig. 7 shows the dust impact rate detected in various amplitude ranges together with the total impact rate. In the 1996–1999 period the highest total impact rate ($3.5 \times 10^{-6} \text{ s}^{-1}$)

was recorded in early 1996 when Ulysses was at rather high ecliptic latitudes ($\beta \sim 50^\circ$) about 3 AU from the Sun. Later, when the spacecraft reached lower latitudes further away from the Sun, the impact rate dropped by about a factor of 3. When Ulysses approached the ecliptic plane the impact rate increased again by a factor of 2 and reached a broad maximum around the aphelion ecliptic plane crossing (at 5.4 AU) in May 1998. The details of the impact rates measured in the various amplitude ranges will be discussed below.

Fig. 8 shows the sensor orientation at the time of a particle impact (rotation angle, top panel). The expected impact directions of interplanetary particles on bound heliocentric orbits (middle panel, Grün et al., 1997) and interstellar particles approaching from the interstellar upstream direction (bottom panel, Witte et al., 1996) are shown for comparison. The intermediate sized and bigger particles (squares, impact charge $Q_i \geq 8 \times 10^{-14}$ C which roughly corresponds to AR2–6) are clearly concentrated towards the interstellar direction. The small particles (crosses, $Q_i \leq 8 \times 10^{-14}$ C roughly corresponding to AR1) do not show such a strong concentration toward certain rotation angles, although many of them are also compatible with the interstellar direction. The particles with the highest ion amplitude ranges (AR4–AR6) are not distinguished in this diagram because they cannot be separated from interstellar particles by directional arguments alone. They have to be distinguished by other means (e.g. mass and speed). In addition, their total number is so small that they constitute only a small ‘contamination’ of the interstellar particles in Fig. 8. The impact direction of the majority of the dust grains detected outside 3 AU is compatible with particles of interstellar origin (bottom panel of Fig. 8).

5.1. Interstellar dust

Interstellar particles are identified by their impact direction and their impact speed: they approach from the same direction as the interstellar gas measured with Ulysses and move on hyperbolic trajectories through the Solar System (Grün et al., 1994; Baguhl et al., 1995a; Witte et al., 1996). In the Ulysses and Galileo data sets they are mostly found in amplitude ranges AR2 and AR3.

The measured impact rate of grains in AR2 and AR3 is shown in the bottom panel of Fig. 7. As in the previous 1993–1995 period the impact rate of these intermediate size grains was relatively constant, except a slight drop after mid-1996. However, on average the impact rate is lower than previously: after 1996 we find an average rate of $\sim 8 \times 10^{-7} \text{ s}^{-1}$ whereas between 1993 and 1995 the rate was $\sim 2 \times 10^{-6} \text{ s}^{-1}$.

Fig. 7 also shows the expected impact rate of interstellar particles assuming that they approach from the direction of interstellar helium (Witte et al., 1996) and that they move through the Solar System on straight trajectories with a relative velocity of 26 km s^{-1} . This assumption means dynam-

ically that radiation pressure cancels gravity for these particles ($\beta = 1$) and that their Larmor radii are large compared with the dimension of the Solar System. Both assumptions are reasonable for particles with masses between 10^{-13} and 10^{-12} g which is the dominant size range measured for interstellar grains (Grün et al., 1997). The variation predicted by the model is caused by changes in the instrument’s viewing direction with respect to the approach direction of the particles and changes in the relative velocity between the spacecraft and the particles. The dust particle flux is independent of heliocentric distance in this simple model, which gives relatively good agreement with the observed impact rate. The assumed flux of oncoming particles at infinity, however, had to be scaled down by a factor of 3 as compared to a value of $1.5 \times 10^{-4} \text{ m}^{-2} \text{ s}^{-1}$ found before 1996 (Grün et al., 1994).

Detailed modelling of the interaction of the dust grains with the heliosphere (Landgraf, 2000) shows that the change of the polarity of the interplanetary magnetic field with the solar cycle imposes a temporal variation of the flux and the spatial distribution of small interstellar dust grains inside the heliosphere (radius smaller than $0.4 \mu\text{m}$): the drop by almost a factor of 3 in the dust flux after mid-1996 is caused by a defocussing effect of the interplanetary magnetic field which effectively prevents small interstellar grains from entering the inner heliosphere. This dynamical model better explains the observed impact rate between 1990 and 2000, including the drop after mid-1996.

The mass distribution of interstellar grains entering the heliosphere is strongly modified by the interaction with the solar radiation field. Radiation pressure is strongly grain size dependent and even exceeds solar gravity for particle masses between about 10^{-16} and 10^{-14} g. Since radiation pressure counteracts solar gravity, the size distribution of interstellar grains gets modified: Ulysses and Galileo measurements between 2 and 4 AU show a depletion in the range 10^{-14} – 3×10^{-13} g (β gap Landgraf et al., 1999). This corresponds to a diameter range 0.2 – $0.6 \mu\text{m}$ for spherical particles with a mass density of 2.5 g cm^{-3} .

5.2. Submicrometre-sized interplanetary dust

The impact rate of the smallest particles (AR1), and the variability of that rate with time, are both much greater than those for the medium-sized AR2 and AR3 particles. Particles at high ecliptic latitudes are attributed to a population of small interplanetary particles on escape trajectories from the Solar System (β -meteoroids, Baguhl et al., 1995b; Hamilton et al., 1996). β -meteoroids have been detected with the Ulysses instrument over the Sun’s poles in 1994 and 1995 (Wehry and Mann, 1999). Due to the detection geometry, however, they became undetectable after mid-1996. This is consistent with the drop in the impact rate by a factor of 10 between January and December 1996 seen in Fig. 7 (see Paper V for the impact rate above the Sun’s poles).

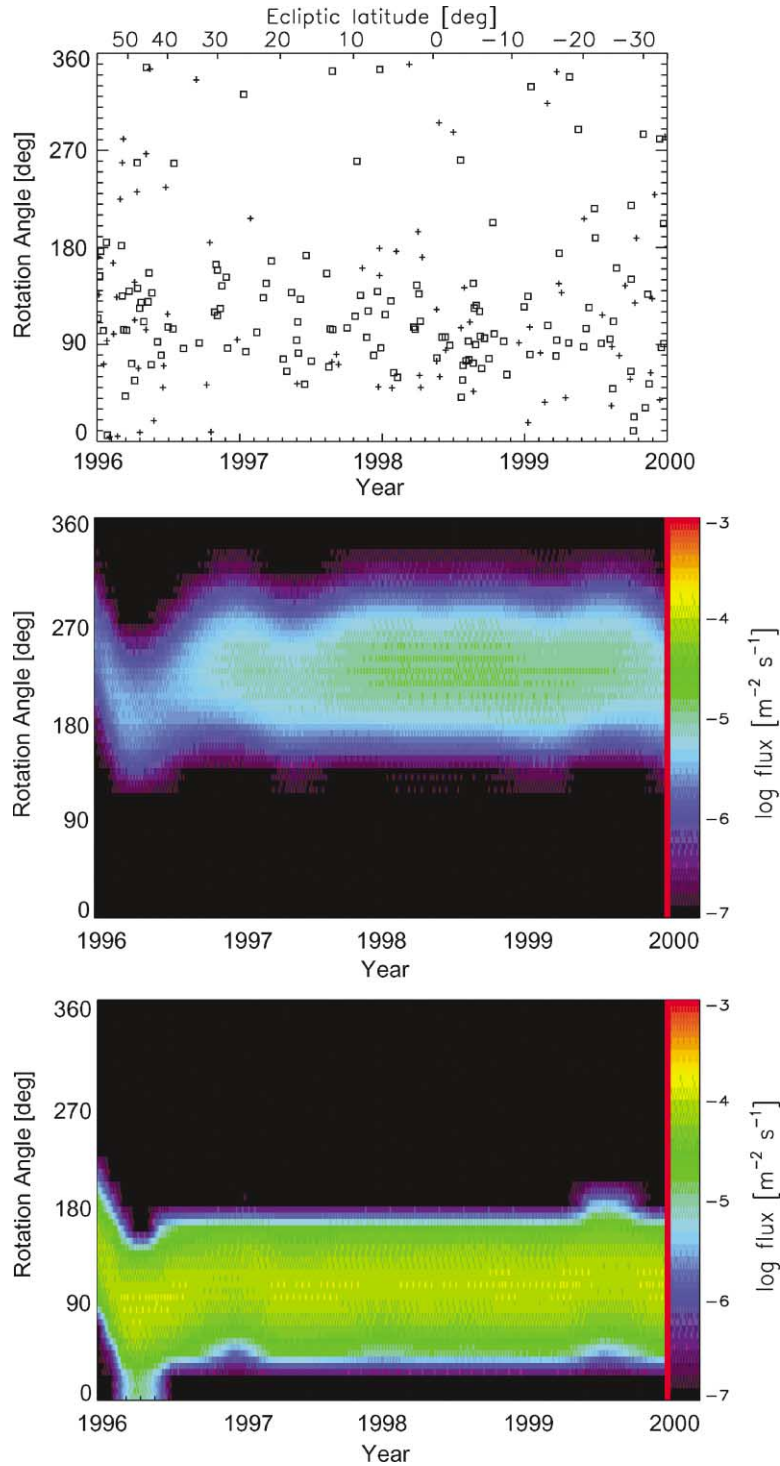


Fig. 8. Rotation angle vs. time. Top panel: all particles detected between 1996 and 1999. Plus signs indicate particles with impact charge $Q_I < 8 \times 10^{-14}$ C, squares those with $Q_I \geq 8 \times 10^{-14}$ C. Ulysses' ecliptic latitude is indicated on the top. Middle panel: expected impact direction for interplanetary particles on heliocentric circular bound orbits concentrated towards the ecliptic plane (Grün et al., 1997). Bottom panel: expected impact direction for interstellar grains approaching from the interstellar upstream direction (Witte et al., 1996). The directions of most of the particles with larger Q_I are consistent with the interstellar upstream direction.

At the aphelion ecliptic plane crossing in 1998 a maximum occurred in the AR1 impact rate while Ulysses was within $\pm 5^\circ$ ecliptic latitude. This is consistent with interplanetary particles concentrated toward the ecliptic plane.

Streams of tiny dust particles were detected with the dust detectors on board Ulysses and Galileo out to a distance of 2 AU from Jupiter (Grün et al., 1993, 1996). These grains originate from the Jovian system (Zook et al., 1996; Grün

et al., 1998; Graps et al., 2000). The dust stream particles impacts occurred only in the lowest amplitude range AR1 (Papers III and IV) and in principle they could contribute to the AR1 rate shown in Fig. 7. From 1996 to 1999, the distance between Jupiter and Ulysses was more than 6 AU (Table 4) and around Ulysses' ecliptic plane crossing in 1998 the distance from Jupiter was 10 AU: Jupiter and Ulysses were on opposite sides of the Solar System and, hence, the Jupiter stream particles could not contribute to the AR1 impacts.

In February 2004, Ulysses will fly by Jupiter within a distance of 0.8 AU. This will again give the opportunity to measure the Jovian dust streams and to test presently existing models. (Note that the masses and velocities for the stream particles given in Papers II and III are not correct, Zook et al., 1996; in reality, the stream particles are smaller and faster than implied by the instrument calibration.)

5.3. Micrometre-sized interplanetary dust; comparison with Pioneer 10 and Pioneer 11 measurements

The impact rate of big particles in AR4–AR6 ($Q_1 > 10^{-10} \text{ C}$) showed a clear maximum at Ulysses' perihelion ecliptic plane crossing in 1995 (heliocentric distance 1.3 AU, Paper V). These impacts were attributed to particles on low inclination heliocentric orbits (Grün et al., 1997). From 1996 to 1999, impacts in AR4–AR6 occurred at a low and relatively constant rate of $1\text{--}2 \times 10^{-7} \text{ s}^{-1}$, except when Ulysses was close to the ecliptic plane ($-5^\circ \lesssim \beta \lesssim 5^\circ$, $\approx 5 \text{ AU}$): in this period the dust detector recorded no impacts at all. Here one has to keep in mind that the statistical uncertainty is very large. In fact, many of the histogram bins for AR4–6 in Fig. 7 represent only one dust impact so that—given the statistical uncertainty—this is still consistent with a dust population concentrated toward the ecliptic plane. However, the measured impact directions of some of these grains are not in agreement with low-inclination circular orbits about the Sun (Fig. 8). The impact directions of $180^\circ \leq \text{ROT} \leq 360^\circ$ rather indicate that the particles moved on highly inclined orbits.

The only spacecraft other than Ulysses and Galileo which were equipped with in situ dust detectors and traversed the outer Solar System were Pioneer 10 and 11. Both dust detectors consisted of an assembly of pressurized cells and a device to monitor the pressure in each cell (Humes, 1980). When a meteoroid penetrated the cell wall, the gas escaped from the cell and the loss of pressure was detected. Once penetrated, a cell was no longer sensitive to meteoroid impacts, which lead to a decrease of the sensor area with time. The only difference between the Pioneer 10 and 11 detectors was that the stainless-steel cell walls were $25 \mu\text{m}$ thick for the Pioneer 10 detector and $50 \mu\text{m}$ thick for the Pioneer 11 detector. This difference in wall thickness provided a differ-

ence in threshold sensitivity of the detectors. The threshold sensitivities for meteoroids with a density of 0.5 g cm^{-3} at impact speeds of 20 km s^{-1} was $8 \times 10^{-10} \text{ g}$ for Pioneer 10 and $6 \times 10^{-9} \text{ g}$ for Pioneer 11, respectively.

Between 3 and 18 AU from the Sun, measurements by the Pioneer 10 detector showed a dust flux of $\approx 3 \times 10^{-6} \text{ m}^{-2} \text{ s}^{-1}$ out to 18 AU (Humes, 1980). At this distance the nitrogen in the pressurized cells froze out and measurements further away from the Sun became impossible. Dust measurements by Pioneer 11 were obtained out to Saturn's orbit. During three passages of Pioneer 11 through the heliocentric distance range from 3.7 to 5 AU the detector observed a roughly constant dust flux between 3×10^{-7} and $2 \times 10^{-6} \text{ m}^{-2} \text{ s}^{-1}$. The absolute value is uncertain because the two measurement channels of the dust instrument gave fluxes which differed by a factor of 5 (Humes, 1980). On Pioneer 10, the second measurement channel of the dust instrument failed immediately after launch, so only one channel remained. Given the Pioneer 11 discrepancy, Pioneer 10 fluxes are also probably uncertain by at least a factor of 5.

The Pioneer 10 and 11 dust measurements led to the conclusion that the dust had to be on highly eccentric orbits with random inclinations rather than circular orbits concentrated towards the ecliptic plane. The distribution of the semi-major axis a was $n(a) \propto a^2$ if the particles were on bound orbits about the Sun (Humes, 1980).

We can compare the dust fluxes reported by Humes (1980) from the Pioneer 10 and 11 measurements between 3 and 5 AU with our Ulysses measurements in the same spatial region. If the inclinations of the dust grains were randomly distributed, Ulysses should have detected these large 'Pioneer' particles independent of the ecliptic latitude of the spacecraft, similar to the interstellar dust grains. Since the interstellar particles form a monodirectional stream approaching from rotation angles $90 \pm 90^\circ$ (Fig. 8), non-interstellar particles approaching from this direction are very difficult to separate. Therefore, we only consider rotation angles $270 \pm 90^\circ$ where no interstellar grains are expected to come from. This corresponds to half a rotation period of Ulysses.

For an isotropic flux of dust grains, the sensor area of the Ulysses dust detector spin-averaged over one hemisphere is about 300 cm^2 . Assuming an isotropic flux of $3 \times 10^{-6} \text{ m}^{-2} \text{ s}^{-1}$ suggested by Pioneer 10, within 4 years of measurement time, Ulysses should have detected about 10 impacts of particles with $m \geq 8 \times 10^{-10} \text{ g}$. Pioneer 11, sensitive to larger particles, predicts that between 1 and 7 particles with $m \geq 6 \times 10^{-9} \text{ g}$ should be found by Ulysses. The Ulysses data in Table 4, however, shows far fewer grains of this size with the right impact direction; only the largest two grains no. 1569 and 1575 with masses of 2×10^{-9} and $5 \times 10^{-8} \text{ g}$, respectively, are sufficiently large. Even after accounting for the factor of 10 (Grün et al., 1995c) uncertainty in the Ulysses mass determination, the Pioneer and Ulysses rates are not in agreement.

The fluxes of large particles in the size range of $\approx 10 \mu\text{m}$ ($m \approx 2 \times 10^{-9} \text{g}$) implied by the Pioneer measurements are not seen by Ulysses.

There are at least three possibilities to explain this discrepancy:

- (A) the calibrations of the Ulysses and Pioneer detectors are not correct by very large factors;
- (B) many of the Pioneer ‘penetrations’ are spurious and not due to actual meteoroid impacts;
- (C) there is a population of meteoroids that can easily be detected with the Pioneer sensors, but not with the Ulysses sensor.

To investigate possibility (A), we can ask which mass threshold of the Ulysses detector we have to assume in order to reproduce the dust fluxes observed by Pioneer 10/11. If we take a mass threshold of $\sim 10^{-13} \text{g}$ we find 12 particles with rotation angles $270 \pm 90^\circ$ and for a threshold of $\sim 10^{-12} \text{g}$ we find five particles in the Ulysses data set. Thus, only if we assume that the mass calibration of either the Ulysses or the Pioneer detectors is wrong by at least 3 orders of magnitude can we match the fluxes observed by Pioneer and by Ulysses.

How do these numbers compare with the earlier data when Ulysses was also at large ecliptic latitudes between Jupiter fly-by in 1992 and the passages above the Sun’s polar regions in 1995? Between mid-1992 and mid-1994 two particles were detected with masses larger than the Pioneer 10 threshold and one particle larger than the Pioneer 11 threshold (Krüger et al., 1999b), whereas 6 and between 0.6 and 4, respectively, should have been detected in order to reproduce the fluxes measured by the Pioneer detectors. Or vice versa, if we vary the detection threshold, the discrepancy is again roughly 3 orders of magnitude.

It should be noted that for Pioneer the calibrated mass of grains that can penetrate the cell walls of the detectors is only valid for impact speeds of $v = 20 \text{ km s}^{-1}$ and grain densities $\rho = 0.5 \text{ g cm}^{-3}$. The threshold mass is roughly proportional to $\rho^{-0.5}$ and $v^{-2.5}$ (Humes, 1980). Thus, an uncertainty in the grain density of a factor of 4 causes a change in the mass threshold of less than a factor of 2. A decrease of the relative speed from 20 km s^{-1} at 1 AU to 10 km s^{-1} at 3–5 AU would increase the mass threshold by more than a factor of 5. Given the speed dependence of the mass threshold of the Ulysses detector which is proportional to $v^{-3.5}$, this would somewhat reduce the order of 3 discrepancy found above.

One might argue that erosion of the cell walls of the Pioneer detectors by particles smaller than the detection threshold has led to a continuous degradation of the detection threshold. The area of each pressurised cell was 24.5 cm^2 whereas sizes of impact craters created by particles of micrometer sizes would have been in the range of a few $10 \mu\text{m}$. Thus, it would need an extremely large number of particle impacts below the threshold until one has a high probability that a particle too small to penetrate the undamaged cell wall

will hit the cell in an eroded region. Given the low number of impacts in interplanetary space, this process is extremely unlikely to happen.

For the Ulysses instrument one should note that the sensor was only calibrated for masses up to 10^{-12}g at impact speeds of 10 km s^{-1} and 10^{-10}g at 2 km s^{-1} , respectively. For larger masses the calibration had to be extrapolated (Grün et al., 1992a). However, the validity of this extrapolation is supported by calibration measurements of the DIDSY instrument on board the Giotto spacecraft (Göller et al., 1987).

Regarding possibility (B) the factor of five discrepancy between the two measurement channels of the Pioneer 11 dust detector is not understood. Furthermore, one channel of the Pioneer 10 instrument failed completely so that only one channel was left. Although, apart from this failure the Pioneer 10 instrument performed very well, the Pioneer 10/11 data should be treated with considerable caution.

For case (C), we have to consider the fields-of-view of the dust detectors on Pioneer 10/11 and on Ulysses: Ulysses has the highest sensitivity for dust particles approaching from a direction more or less perpendicular to the spacecraft–Earth line whereas the Pioneer detectors have the highest sensitivity for grains approaching along the spacecraft–Earth line from the anti–Earth direction. Because of these very different detection geometries, Pioneer 10/11 may have detected dust grains on highly eccentric heliocentric orbits which were hardly detectable with Ulysses. In addition, the field-of-view of the Ulysses detector is 140° and that of the Pioneer detector arrays is more than 180° (Humes, 1980). Depending on the distribution of the orbital elements of the grains this can lead to significant differences in the detected fluxes. For an incident isotropic flux the expected difference is only about a factor of 2, whereas for particles on more or less radial heliocentric trajectories the difference may be much larger: grains approaching the Sun on highly eccentric orbits are easily detected with the Pioneer detectors but hardly with Ulysses.

The Pioneer 10 and 11 spacecraft also carried photopolarimeters on board which were used to map the zodiacal light and background starlight during the cruise to Jupiter in two optical bandpasses at 0.44 and $0.64 \mu\text{m}$. Beyond the asteroid belt no decrease in brightness with distance was detected, indicating that the spacecraft were beyond the main zodiacal dust cloud and that the background starlight was directly measured. Only if the dust particles were darker than cometary dust grains could the measured brightnesses explain the in situ dust fluxes (Kneissel and Mann, 1990).

It should also be noted that Pioneer 10 and 11 detected a few dust impacts during Jupiter fly-by (Humes, 1976). A more detailed analysis of these measurements may lead to clarification of the discrepancy between Ulysses and Pioneer 10/11 discussed here.

What is the source of interplanetary dust grains in the outer Solar System? A significant source for interplanetary dust probably lies beyond Neptune’s orbit: mutual collisions

between Edgeworth–Kuiper belt objects (EKOs) plays a significant role as a dust production mechanism (Stern, 1996). Impacts of interstellar grains onto the surfaces of (EKOs) may also lead to significant secondary dust ejection (Yamamoto and Mukai, 1998). Once released from their parent bodies the grains spiral towards the Sun under Poynting–Robertson and solar wind drags and may even reach Earth (Liou et al., 1996). Particles several micrometre in radius are most efficiently transported towards the Sun. Such grains should show up in AR4-6 in the Ulysses data. They should, however, show a flux increase towards the ecliptic plane. Another dust source in the outer Solar System are long period comets. The particles they release into interplanetary space should move on highly inclined orbits with random inclinations. In principle, such grains can support the interpretation that the grains detected by the Pioneer detectors move on highly eccentric orbits, although the flux should increase towards the inner Solar System which is not seen. It should be noted that Ulysses also detected impacts of big particles at high ecliptic latitudes above the Sun's polar regions (Krüger et al., 1999b) which are compatible with highly inclined orbits. Detailed modelling of the dust environment in the outer Solar System including an investigation of different possible source types is forthcoming (Landgraf et al., in prep.). The region between Jupiter and Saturn will be traversed by the Cassini spacecraft between 2001 and 2004 and the dust distribution will be measured with the Cosmic Dust Analyser carried on board (Srama et al., 2001). Together with modelling of the dust dynamics this will hopefully improve our understanding of the interplanetary dust complex beyond the asteroid belt.

6. Summary

In this paper, which is the seventh in a series of Ulysses and Galileo papers, we present data from the Ulysses dust instrument for the period January 1996–December 1999 when Ulysses was traversing interplanetary space between 3 and 5 AU from the Sun at ecliptic latitudes between $+50^\circ$ and -35° . A total number of 218 dust impacts has been recorded during this period. Together with 1477 impacts recorded in interplanetary space and near Jupiter between Ulysses' launch in October 1990 and December 1995 (Grün et al., 1995a; Krüger et al., 1999b), the complete data set of dust

impacts measured with the Ulysses dust detector so far comprises 1695 impacts.

A relatively constant impact rate of 0.2 dust impacts per day was detected during the whole 4-year time span. Most of these particles were of interstellar origin, a minor fraction being interplanetary particles.

The flux measured with the Ulysses detector has been compared with the dust measurements obtained with the Pioneer 10 and 11 detectors beyond 3 AU heliocentric distance (Humes, 1980). The flux of particles with $m \geq 10^{-9}$ g as measured with Ulysses is about a factor of 5 lower than expected from the Pioneer 10/11 measurements. Although we are dealing with only a small number of impacts, the most plausible explanations are (a) the mass calibrations of the Ulysses and/or Pioneer detectors for $\approx 10 \mu\text{m}$ grains differ by up to 3 orders of magnitude; (b) many of the Pioneer detections are spurious and not due to actual meteoroid impacts; (c) the dust grains detected by Pioneer belong to a population of dust which could not or only partially be detected with Ulysses.

Noise tests performed regularly during the 4 year period showed a degradation in the noise sensitivity of the dust instrument which is caused by a reduction in the channeltron amplification. This, however, has no effect on the interpretation of the present data set.

Acknowledgements

We thank the Ulysses project at ESA and NASA/JPL for effective and successful mission operations. Our referees, Alexander V. Krivov and Larry W. Esposito, provided valuable suggestions which improved the presentation of our results. This work has been supported by the Deutsches Zentrum für Luft-und Raumfahrt e.V. (DLR).

Appendix

Conversion of impact charge, particle mass and particle radius for dust grains of different sizes and impact speeds (Table 5). Assuming spherical homogeneous particles with a density of $\rho = 2 \text{ g cm}^{-3}$, the grain radius can be directly calculated from the grain mass ($m = 4\pi/3\rho r^3$, column 2). The impact charge created when a dust particle with the

Table 5

Mass (g)	Radius (μm)	Impact charge Q_i		Amplitude range	
		$v = 5 \text{ km s}^{-1}$ (C) (3)	$v = 23 \text{ km s}^{-1}$ (C) (4)	$v = 5 \text{ km s}^{-1}$ (5)	$v = 23 \text{ km s}^{-1}$ (6)
1.2×10^{-14}	0.1	3.6×10^{-16}	3.2×10^{-14}	—	AR1
1.7×10^{-13}	0.2	5.0×10^{-15}	4.5×10^{-13}	—	AR2
1.9×10^{-12}	0.6	6.0×10^{-14}	5.0×10^{-12}	AR1	AR3
1.7×10^{-11}	1.2	5.1×10^{-13}	4.6×10^{-11}	AR2	AR4
1.5×10^{-10}	2.6	4.4×10^{-12}	4.0×10^{-10}	AR3	AR5

mass given in column (1) hits the detector target (columns 3 and 4) has been derived from the instrument calibration published by Grün et al. (1995a–c), their Fig. 3a). The conversion between particle mass and ion charge amplitude range AR (columns 5 and 6) has been taken from Fig. 4 of the same publication. The impact charge and the corresponding amplitude range depend on the particle's impact speed. Values are given for two different speeds (5 and 23 km s⁻¹, respectively). It should be noted that the Ulysses and Galileo dust instruments could only be calibrated in the laboratory up to masses of 10⁻¹² g at impact speeds of 10 km s⁻¹ and up to 10⁻¹⁰ g at impact speeds of 2 km s⁻¹, respectively. For larger masses the calibration had to be extrapolated (Grün et al., 1992a). The validity of this extrapolation, however, is supported by calibration measurements for other dust instruments (Göller et al., 1987)

References

- Baggaley, W.J., 2000. Advanced Meteor Orbit Radar observations of interstellar meteoroids. *J. Geophys. Res.* 105 (A5), 10,353–10,361.
- Baguhl, M., Grün, E., Hamilton, D.P., Linkert, G., Riemann, R., Staubach, P., 1995a. The flux of interstellar dust observed by Ulysses and Galileo. *Space Sci. Rev.* 72, 471–476.
- Baguhl, M., Grün, E., Linkert, G., Linkert, D., Siddique, N., 1993. Identification of 'small' dust impacts in the Ulysses dust detector data. *Planet. Space Sci.* 41, 1085–1098.
- Baguhl, M., Hamilton, D.P., Grün, E., Dermott, S.F., Fechtig, H., Hanner, M.S., Kissel, J., Lindblad, B.A., Linkert, D., Linkert, G., Mann, I., McDonnell, J.A.M., Morfill, G.E., Polansky, C., Riemann, R., Schwehm, G., Staubach, P., Zook, H.A., 1995b. Dust measurements at high ecliptic latitudes. *Science* 268, 1016–1020.
- Balogh, A., Marsden, R., Smith, E.E., 2001. *The Heliosphere Near Solar Minimum: The Ulysses Perspective*. Springer Praxis, Springer, Berlin.
- Divine, N., 1993. Five populations of interplanetary meteoroids. *J. Geophys. Res.* 98, 17,029–17,048.
- Frisch, P.C., Dorschner, J., Geiß, J., Greenberg, J.M., Grün, E., Landgraf, M., Hoppe, P., Jones, A.P., Krättschmer, W., Linde, T.J., Morfill, G.E., Reach, W.T., Slavin, J., Svestka, J., Witt, A., Zank, G.P., 1999. Dust in the local interstellar wind. *Astrophys. J.* 525, 492–516.
- Göller, J.R., Grün, E., Maas, D., 1987. Calibration of the DIDSY-IPM dust detector and application to other impact ionisation detectors on board the P/Halley probes. *Astron. Astrophys.* 187, 693–698.
- Graps, A.L., Grün, E., Svedhem, H., Krüger, H., Horányi, M., Heck, A., Lammers, S., 2000. Io as a source of the Jovian dust streams. *Nature* 405, 48–50.
- Grün, E., Baguhl, M., Divine, N., Fechtig, H., Hamilton, D.P., Hanner, M.S., Kissel, J., Lindblad, B.A., Linkert, D., Linkert, G., Mann, I., McDonnell, J.A.M., Morfill, G.E., Polansky, C., Riemann, R., Schwehm, G., Siddique, N., Staubach, P., Zook, H.A., 1995a. Two years of Ulysses dust data. *Planet. Space Sci.* 43, 971–999, Paper III.
- Grün, E., Baguhl, M., Divine, N., Fechtig, H., Hamilton, D.P., Hanner, M.S., Kissel, J., Lindblad, B.A., Linkert, D., Linkert, G., Mann, I., McDonnell, J.A.M., Morfill, G.E., Polansky, C., Riemann, R., Schwehm, G., Siddique, N., Staubach, P., Zook, H.A., 1995b. Three years of Galileo dust data. *Planet. Space Sci.* 43, 953–969, Paper II.
- Grün, E., Baguhl, M., Hamilton, D.P., Kissel, J., Linkert, D., Linkert, G., Riemann, R., 1995c. Reduction of Galileo and Ulysses dust data. *Planet. Space Sci.* 43, 941–951, Paper I.
- Grün, E., Baguhl, M., Hamilton, D.P., Riemann, R., Zook, H.A., Dermott, S., Fechtig, H., Gustafson, B.A., Hanner, M.S., Horányi, M., Khurana, K.K., Kissel, J., Kivelson, M., Lindblad, B.A., Linkert, D., Linkert, G., Mann, I., McDonnell, J.A.M., Morfill, G.E., Polansky, C., Schwehm, G., Srama, R., 1996. Constraints from Galileo observations on the origin of jovian dust streams. *Nature* 381, 395–398.
- Grün, E., Fechtig, H., Hanner, M.S., Kissel, J., Lindblad, B.A., Linkert, D., Maas, D., Morfill, G.E., Zook, H.A., 1992a. The Galileo dust detector. *Space Sci. Rev.* 60, 317–340.
- Grün, E., Fechtig, H., Kissel, J., Linkert, D., Maas, D., McDonnell, J.A.M., Morfill, G.E., Schwehm, G., Zook, H.A., Giese, R.H., 1992b. The Ulysses dust experiment. *Astron. Astrophys. Suppl. Ser.* 92, 411–423.
- Grün, E., Gustafson, B.E., Mann, I., Baguhl, M., Morfill, G.E., Staubach, P.A.T., Zook, H.A., 1994. Interstellar dust in the heliosphere. *Astron. Astrophys.* 286, 915–924.
- Grün, E., Krüger, H., Graps, A., Hamilton, D.P., Heck, A., Linkert, G., Zook, H., Dermott, S., Fechtig, H., Gustafson, B., Hanner, M., Horányi, M., Kissel, J., Lindblad, B., Linkert, G., Mann, I., McDonnell, J.A.M., Morfill, G.E., Polansky, C., Schwehm, G., Srama, R., 1998. Galileo observes electromagnetically coupled dust in the jovian magnetosphere. *J. Geophys. Res.* 103, 20,011–20,022.
- Grün, E., Krüger, H., Landgraf, M., 2001. In: Balogh, A., Marsden, R., Smith, E. (Eds.), *The Heliosphere at Solar Minimum: The Ulysses Perspective*. Springer Praxis, Berlin, in press.
- Grün, E., Landgraf, M., 2000. Collisional consequences of big interstellar grains. *J. Geophys. Res.* 105 (A5), 10,291–10,298.
- Grün, E., Staubach, P., Baguhl, M., Hamilton, D.P., Zook, H.A., Dermott, S., Gustafson, B.A., Fechtig, H., Kissel, J., Linkert, D., Linkert, G., Srama, R., Hanner, M.S., Polansky, C., Horányi, M., Lindblad, B.A., Mann, I., McDonnell, J.A.M., Morfill, G.E., Schwehm, G., 1997. South-north and radial traverses through the interplanetary dust cloud. *Icarus* 129, 270–288.
- Grün, E., Zook, H.A., Baguhl, M., Balogh, A., Bame, S.J., Fechtig, H., Forsyth, R., Hanner, M.S., Horányi, M., Kissel, J., Lindblad, B.A., Linkert, D., Linkert, G., Mann, I., McDonnell, J.A.M., Morfill, G.E., Phillips, J.L., Polansky, C., Schwehm, G., Siddique, N., Staubach, P., Svestka, J., Taylor, A., 1993. Discovery of Jovian dust streams and interstellar grains by the Ulysses spacecraft. *Nature* 362, 428–430.
- Hamilton, D.P., Burns, J.A., 1993. Ejection of dust from Jupiter's gossamer ring. *Nature* 364, 695–699.
- Hamilton, D.P., Grün, E., Baguhl, M., 1996. In: Gustafson, B.A.S., Hanner, M.S. (Eds.), *Physics, Chemistry and Dynamics of Interplanetary Dust*. ASP Conference Series, Vol. 104, pp. 31–34.
- Horányi, M., Grün, E., Heck, A., 1997. Modeling the Galileo dust measurements at Jupiter. *Geophys. Res. Lett.* 24, 2175–2178.
- Horányi, M., Morfill, G., Grün, E., 1993. Mechanism for the acceleration and ejection of dust grains from Jupiter's magnetosphere. *Nature* 363, 144–146.
- Humes, D.H., 1976. In: Gehrels, T. (Ed.), *Jupiter*. University of Arizona Press, Tucson, pp. 1052–1067.
- Humes, D.H., 1980. Results of Pioneer 10 and 11 meteoroid experiments: interplanetary and near-Saturn. *J. Geophys. Res.* 85, 5841–5852.
- Kneissel, B., Mann, I., 1990. Three-dimensional models of the global zodiacal dust cloud—A bimodal model of the solar dust heliosphere. In: *Physics of the Outer Heliosphere*. Proceedings of the 1st COSPAR Colloquium, Warsaw, Poland, Pergamon Press, 1990, pp. 93–95.
- Krüger, H., Grün, E., Graps, A., Bindschadler, D., Dermott, S., Fechtig, H., Gustafson, B.A., Hamilton, D.P., Hanner, M.S., Horányi, M., Kissel, J., Lindblad, B., Linkert, D., Linkert, G., Mann, I., McDonnell, J.A.M., Morfill, G.E., Polansky, C., Schwehm, G., Srama, R., Zook, H., 2001. One year of Galileo dust data: 1996. *Planet. Space Sci.* (this issue).
- Krüger, H., Grün, E., Hamilton, D.P., Baguhl, M., Dermott, S., Fechtig, H., Gustafson, B.A., Hanner, M.S., Horányi, M., Kissel, J., Lindblad, B.A., Linkert, D., Linkert, G., Mann, I., McDonnell, J.A.M., Morfill, G.E., Polansky, C., Riemann, R., Schwehm, G., Srama, R., Zook, H., 1999a. Three years of Galileo dust data: II. 1993 to 1995. *Planet. Space Sci.* 47, 85–106, Paper IV.
- Krüger, H., Grün, E., Landgraf, M., Baguhl, M., Dermott, S., Fechtig, H., Gustafson, B.A., Hamilton, D.P., Hanner, M.S., Horányi, M., Kissel, J., Lindblad, B., Linkert, D., Linkert, G., Mann, I., McDonnell, J.A.M., Morfill, G.E., Polansky, C., Schwehm, G., Srama, R., Zook, H.,

- 1999b. Three years of Ulysses dust data: 1993 to 1995, *Planet. Space Sci.* 47, 363–383, Paper V.
- Landgraf, M., 2000. Modelling the motion and distribution of interstellar dust inside the heliosphere. *J. Geophys. Res.* 105 (A5), 10,303–10,316.
- Landgraf, M., Augustsson, K., Grün, E., Gustafson, B.A.S., 1999. Deflection of the local interstellar dust flow by solar radiation pressure. *Science* 286, 2319–2322.
- Landgraf, M., Baggeley, W.J., Grün, E., Krüger, H., Linkert, G., 2000. Aspects of the mass distribution of interstellar dust grains in the Solar System from in situ measurements. *J. Geophys. Res.* 105 (A5), 10,343–10,352.
- Liou, J.-C., Zook, H.A., Dermott, S.F., 1996. Kuiper Belt dust grains as a source of interplanetary dust particles. *Icarus* 124, 429–440.
- Mann, I., Grün, E., Wilck, M., 1996. The contribution of asteroid dust to the interplanetary dust cloud: the impact of ULYSSES results on the understanding of dust production in the asteroid belt and of the formation of the IRAS dust bands. *Icarus* 120, 399–407.
- Mann, I., Kimura, H., 2000. Interstellar dust properties derived from mass density, mass distribution, and flux rates in the heliosphere. *J. Geophys. Res.* 105 (A5), 10,317–10,328.
- Srama, R., Bradley, J.G., Grün, E., Ahrens, T.J., Auer, S., Cruise, M., Fechtig, H., Graps, A., Havnes, O., Heck, A., Helfert, S., Igenbergs, E., Jeßberger, E.K., Johnson, T.V., Kempf, S., Krüger, H., Lamy, P., Landgraf, M., Linkert, D., Lura, F., McDonnell, J.A.M., Möhlmann, D., Morfill, G.E., Schwehm, G.H., Stübig, M., Svestka, J., Tuzzolino, A.J., Wäsch, R., Zook, H.A., 2001. The Cassini cosmic dust analyzer. *Space Sci. Rev.*, submitted.
- Stern, S.A., 1996. Signatures of collisions in the Kuiper disk. *Astron. Astrophys.* 310, 999–1010.
- Stone, R.G., Bougeret, J.L., Caldwell, J., Canu, P., de Conchy, Y., Cornilleau-Wehrin, N., Desch, M.D., Fainberg, J., Goetz, K., Goldstein, M.L., Harvey, C.C., Hoang, S., Howard, R., Kaiser, M.L., Kellogg, P., Klein, B., Knoll, R., Lecacheux, A., Langyel-Frey, D., MacDowall, R.J., Manning, R., Meetre, C.A., Meyer, A., Monge, N., Monson, S., Nicol, G., Reiner, M.J., Steinert, J.L., Torres, E., de Villedary, C., Wouters, F., Zarka, P., 1992. The unified radio and plasma wave investigation. *Astron. Astrophys. Suppl. Ser.* 92, 291–316.
- Svestka, J., Auer, S., Baguhl, M., Grün, E., 1996. In: Gustafson, B.A., Hanner, M.S. (Eds.), *Physics, Chemistry and Dynamics of Interplanetary Dust*, Vol. 104, ASP Conference Series, pp. 31–34.
- Taylor, A.D., Baggeley, W.J., Steel, D.I., 1996. Discovery of interstellar dust entering the Earth's atmosphere. *Nature* 380, 323–325.
- Wehry, A., Mann, I., 1999. Identification of β -meteoroids from measurements of the dust detector onboard the Ulysses spacecraft. *Astron. Astrophys.* 341, 296–303.
- Wenzel, K., Marsden, R., Page, D., Smith, E., 1992. The Ulysses mission. *Astron. Astrophys. Suppl. Ser.* 92, 207–219.
- Witte, M., Banaszkiwicz, H., Rosenbauer, H., 1996. Recent results on the parameters of interstellar helium from the Ulysses/GAS experiment. *Space Sci. Rev.* 78 (1/2), 289–296.
- Yamamoto, S., Mukai, T., 1998. Dust production by impacts of interstellar dust on Edgeworth–Kuiper belt objects. *Astron. Astrophys.* 329, 785–791.
- Zook, H., Grün, E., Baguhl, M., Hamilton, D.P., Linkert, G., Linkert, D., Liou, J.-C., Forsyth, R., Phillips, J.L., 1996. Solar wind magnetic field bending of Jovian dust trajectories. *Science* 274, 1501–1503.